Theory and Practice of Electron Transfer within Protein–Protein Complexes: Application to the Multidomain Binding of Cytochrome *c* by Cytochrome *c* Peroxidase

Judith M. Nocek,[†] Jian S. Zhou,[†] Sarah De Forest,[‡] Satyam Priyadarshy,[‡] David N. Beratan,[‡] José N. Onuchic,[§] and Brian M. Hoffman*[,†]

Department of Chemistry, Northwestern University, Evanston, Illinois 60208, Department of Chemistry, University of Pittsburgh, Pittsburgh, Pennsylvania 15260, and Department of Physics, University of California at San Diego, LaJolla, California 92093-0319

Received June 10, 1996 (Revised Manuscript Received August 28, 1996)

Contents

I. Introduction 2459
II. Photoinitiated ET—Experimental Approaches 2460
III. Multisite and Multidomain Binding: Microscopic vs Thermodynamic Constants 2462
  A. 1:1 Stoichiometry 2462
  B. 2:1 Stoichiometry 2464
IV. Quenching as a "4-D" Experiment 2465
  A. Conventional Titrations (C_N and C_R) with 1:1 Stoichiometry 2466
  B. Conventional (C) Titrations with 2:1 Stoichiometry 2467
  C. Inverse Titrations (I_N and I_R) 2469
V. Unimolecular and Bimolecular Electron Transfer in Biomolecules 2470
  A. The Tunneling Pathway Model of Protein Mediated Electron Transfer 2470
  B. Functional Docking 2472
  C. Classical Electrostatics and the Encounter Surface 2473
VI. ET between the Physiological Partners, C*c* and C*c*P 2473
  A. One Structure for the [C*c*P, C*c*] Complex? 2474
  B. Dynamic View—Experimental Evidence for Multiple Conformations 2476
  C. New Titration Strategies Show That C*c*P Has Two Binding Domains 2476
  D. Interactions between the Two C*c*P Binding Domains? 2479
  E. Independent Confirmations of 2:1 Stoichiometry 2481
  F. Kinetic and Physical Characterization of Site-Specific Mutants of C*c*P 2482
  G. Surface Coupling Maps and Electrostatic Maps of the [C*c*P, C*c*] Complex 2484
VII. Discussion 2486

I. Introduction

Studies of long-range electron transfer (LRET) in systems where the redox partners are held at a fixed and rigid distance and orientation have achieved a central role in modern chemistry.[1−14] The paradigmatic system in nature is the photosynthetic reaction center.[2] Three levels of experimental design have been developed to study ET in an environment amenable to synthetic and physical control: linked donor−acceptor model compounds,[3,4] redox-modified proteins,[5,11−13] and modified protein−protein complexes.[6−8,14] In the first level, the ET process necessarily takes place through a covalent and/or H-bonded pathway amenable to changes in distance and composition. The second level, where a redox-active inorganic complex is covalently attached to a surface amino acid residue of a redox protein, introduces the full complexity of intraprotein ET between centers covalently linked to well-defined sites *within* a protein. This raises such issues as the relative importance of "pathways" that involve through-space vs through-bond coupling, with the latter subdividing into covalent bonds and hydrogen bonds.[9] As a variant on this approach, mixed-metal hemoglobin hybrids exhibit intersubunit ET[10] and thus necessarily introduce the issue of ET across a noncovalent protein−protein interface, but do so in a context where the intersubunit contacts and potential ET pathways are structurally well-defined.

This review focuses on the study of ET between proteins that form noncovalent complexes, a higher order problem that introduces additional complexities not seen in the other systems and not fully appreciated when the current interest in LRET began.[15,16] In the study of physiological protein−protein complexes such as that between yeast cytochrome *c* peroxidase (C*c*P) and cytochrome *c* (C*c*),[6,7,14,17] one begins without certain knowledge of the stoichiometry of binding, much less the site or sites on the protein surfaces where binding occurs, and without knowledge of the rules for protein−protein recognition and conformational interconversion that might control the ET process! The ET event occurs within a protein−protein complex across a dynamic protein−protein interface, and as a consequence, the observed kinetics may depend not only on the ET process itself but also on the extent and stoichiometry of binding, as well as on the interfacial dynamics of docking. In short, as we[18,19] and others[20−22] have come to recognize, the first stage in the study of such interprotein ET does not involve the *study* of ET, but rather the *use* of ET measurements to study the stoichiometry and geometry of equilibrium binding as well as the dynamics of docking rearrangements. Only after successes in this stage of the enterprise does one

[†] Northwestern University.
[‡] University of Pittsburgh.
[§] University of California.

S0009-2665(95)00044-6 CCC: $25.00

Judith M. Nocek graduated from Illinois Benedictine College, earning B.S. degrees in Chemistry and Mathematics. In 1986, she completed her Ph.D. studies at Iowa State University under the direction of Donald Kurtz. After performing postdoctoral research at Northwestern University with Brian Hoffman, she has continued at Northwestern University as a Research Associate. Her current research interests include protein–protein interactions and electron transport.

Jian S. Zhou received his B.S. degree from Anhui Normal University (P.R. of China) and his Ph.D. degree from Universite Pierre et Marie Curie (Paris, France) in the field of surface and colloid science. After postdoctoral studies at Bowling Green State University and then Iowa State University, he joined Professor Brian M. Hoffman of Northwestern University in 1993 as a postdoctoral research fellow. His research interests are in electron transfer and in the development and application of biomimetic materials.

Sarah de Forest began her undergraduate studies at the Community College of Philadelphia and she obtained her B.S. at the University of Pittsburgh in 1994. After graduating, she worked for a year with Professor David Beratan at Pitt, studying electron transfer and protein docking. She is currently pursuing a doctoral degree at the University of California, Berkeley, where she is working with Professor Martin Head-Gordon. Her current studies focus on electronic excited states, with an eye toward developing methods to treat large molecular systems.

Satyam Priyadarshy received his M.S. in 1984 from Agra University, Agra, India, and Ph.D. from the Indian Institute of Technology, Bombay (Mumbai) in 1990, working with Professor Sambhu N. Datta. After completing his Ph.D., he worked on rotational relaxation of molecular systems, with Dr. Petr Harrowell at the Physical and Theoretical Chemistry Department, University of Sydney, Sydney, Australia. His second postdoctoral position was with Professor David Beratan at the Department of Chemistry, University of Pittsburgh. There, the work was mostly on long-range electron transfer in biomolecules and on nonlinear optics. Since January 1996, he has been a Research Assistant Professor of Chemistry at the University of Pittsburgh. His current research interests include theoretical studies of exciton dynamics in photosynthetic systems, applications of quantum mechanical methods to advanced materials design, biomolecular processes, and nonlinear optics. Also of interest is the development of efficient self-consistent Hartree–Fock codes for parallel and vector computers.

achieve the ability to ask meaningful questions about the ET event itself.

The current era of studying electron transfer between proteins originated with the recognition that mixing experiments cannot achieve the time resolution needed for in-depth analysis.[23−26] Section II briefly discusses the strategies developed to generalize the use of laser-flash techniques to initiate electron-transfer processes. Section III recounts the fundamental concepts needed to use kinetic measurements to obtain stoichiometric information about protein−protein binding and to obtain information about docking dynamics. Section IV begins the heart of the review. It presents a new "multidimensional" approach to performing measurements of excited-state quenching, one that has broadened and strengthened the application of this venerable technique. Section V summarizes pathways models for the calculation of ET rate constants and their application to bimolecular ET and discusses their combined use with classical electrostatics calculations to understand "functional docking". In section VI, these various issues are illustrated by describing the discovery of multidomain (2:1) binding of C*c* by C*c*P and by a discussion of the ET reactivity within the complexes of C*c* with C*c*P. Finally, a preliminary integration of these efforts is discussed in section VII.

II. Photoinitiated ET−Experimental Approaches

Laser-photolysis methods were introduced to the study of protein−protein binding and *inter*protein electron transfer when it was recognized that replacement of the heme (FeP) of one protein partner by a closed-shell metalloporphyrin, MP (M = Zn or Mg; P = protoporphyrin IX), introduces the possibility of studying photoinitiated electron transfer between the MP and the redox group in the part-

David Beratan received a B.S. in chemistry from Duke University in 1980. After completing his Ph.D. in 1985 with J. J. Hopfield in the Department of Chemistry at Caltech, he moved to the Jet Propulsion Laboratory in Pasadena, CA, as a National Research Council postdoctoral associate. He spent seven years at JPL, the later five as a Member of the Technical Staff. At JPL, he and Onuchic developed the Pathway model for analyzing protein electron-transfer reactions. He also devised new strategies for improving nonlinear optical materials and molecular-scale electronic devices. Beratan was a Visiting Associate in Chemistry at Caltech's Beckman Institute during his last few years in Pasadena. Since 1992, he has been an Associate Professor of Chemistry at the University of Pittsburgh. His current research interests include electron transfer in proteins and DNA, inverse design of materials, and the electronic structure of macromolecules. He currently holds a National Science Foundation National Young Investigator Award.

José Nelson Onuchic received a B.S. in Electrical Engineering in 1980, a B.S. in Physics in 1981, and a M.S. in Applied Physics in 1982 from the University of São Paulo at São Carlos, Brazil. He received his Ph.D. from Caltech in 1987 under the supervision of John J. Hopfield. His thesis work was on new aspects of the theory of electron-transfer reactions in biology. He then spent six months at the Institute for Theoretical Physics in Santa Barbara before returning to Brazil at the University of São Paulo as an Assistant Professor. During his two and one-half years there, he continued his work on electron-transfer theory, on the theory of chemical reactions in the condensed phase, and on molecular electronics. He joined the faculty of the University of California at San Diego in 1990, where he has been working on electron transfer in proteins and other biological and chemical systems, and on the protein-folding problem. In 1992 he received a Beckman Young Investigator Award and he was elected a Fellow of the American Physical Society in 1995.

ner.[7,27,28] A reversible electron transfer cycle within such metal-substituted complexes can be initiated by a laser flash. Photoexcitation of the closed-shell MP substituted into a hemoprotein produces an excited singlet state that rapidly (and generally with high yield) crosses to a long-lived (typically milliseconds), triplet excited state (^{3}MP). The ^{3}MP is a strong reductant and in the presence of a redox-active partner protein, commonly (but not necessarily) one

Brian M. Hoffman earned a S.B. degree at the University of Chicago and a Ph.D. degree from Caltech (with Harden McConnell). After a postdoctoral year at MIT (with Alex Rich) he joined the faculty at Northwestern University in 1967, where he holds a joint appointment in the Department of Chemistry and in the BMBCB department. In addition to his interest in electron transfer, his group employs electron–nuclear double resonance spectroscopy (ENDOR) to study metalloenzyme active-site structure and function and prepares new multimetallic porphyrazine macrocycles. He and his wife Janet boast of four daughters, Tara, Abby, Alexandra, and Julia.

containing a ferriheme, the ^{3}MP is quenched by long-range, intracomplex ET (eq 1).

$$^3\mathrm{MP} + \mathrm{Fe^{3+}P} \rightarrow \mathrm{MP^+} + \mathrm{Fe^{2+}P} \qquad (1)$$

Direct photoexcitation eliminates complications arising from the use of an external reductant, and the MP-substituted metalloprotein can be mixed with its partner protein to preform the ET-competent complex. The resulting charge-separated intermediate (**I**) returns to the ground state by thermally activated ET from $Fe^{2+}P$ to the porphyrin-centered π-cation radical (MP^+) according to eq 2.

$$\mathrm{MP^+} + \mathrm{Fe^{2+}P} \rightarrow \mathrm{MP} + \mathrm{Fe^{3+}P} \qquad (2)$$

In studies of the photoprocess, both transient absorption and emission techniques are used to monitor the kinetic progress curves of ^{3}MP, from which the rate constant for reaction 1 is obtained. To study the thermal ET return (reaction 2) only absorption techniques are applicable.

Heme replacement is a valid method to the extent that the modified protein is a structurally faithful, ET-active analogue of the native hemoprotein. Many studies have addressed this issue and in doing so have fully validated the replacement procedure. Thus, the structure of MgHb, in which all four ferroheme prosthetic groups of hemoglobin are replaced by MgP has been determined crystallographically at 2 Å, and its structure was found to be "indistinguishable" from the native protein at this resolution (Figure II.1).[29] Likewise, NMR studies with Zn*Cc* in aqueous solution[30,31] have demonstrated that the conformation (and ligation state) of C*c* is unchanged by incorporation of Zn^{2+} in place of Fe^{2+}. Similar findings have been reported for Cu[32] and Co-substituted C*c*.[30] In all cases, these studies have overwhelmingly shown that closed-shell metalloproteins are faithful structural analogues of their native proteins in the valence state corresponding to that of the replacement metal ion.

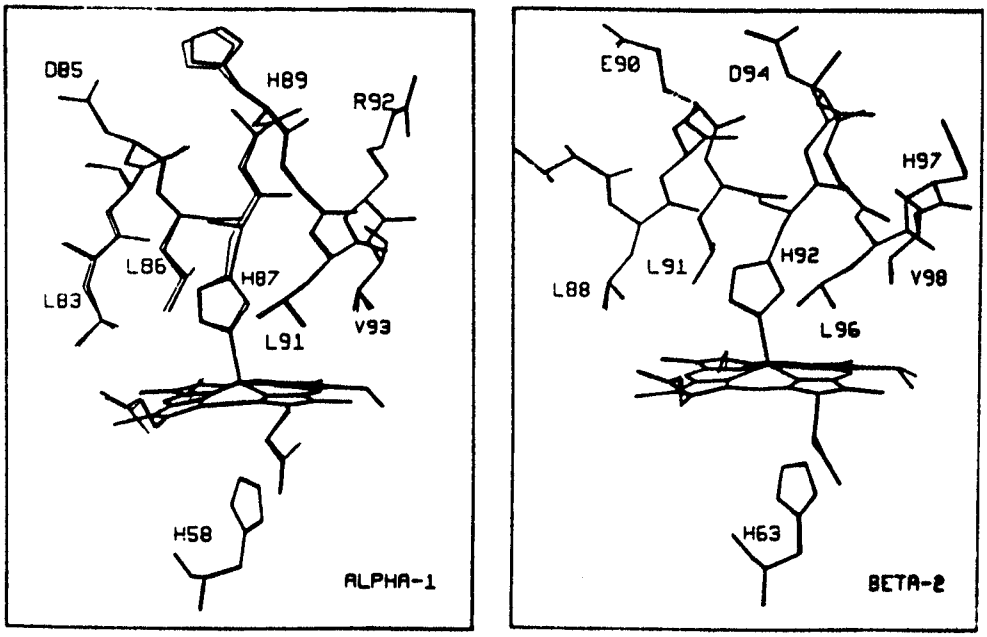

Figure II.1. Superposition of the MgHb (thin lines) and deoxyHb (thick lines) structures in the regions of the α_1 and β_2 heme pockets.

The approach of covalently attaching a photoactive inorganic redox complex to a specific surface amino acid residue of a redox-active protein, which revolutionized the study of intraprotein ET,[5,11−13] has been extended recently to the study of interprotein ET between redox centers in noncovalent protein−protein complexes.[33,34] In this procedure, a laser flash causes a metal complex (Ru^{2+}) bound to the outside of a redox protein (e.g., C*c*) to exchange an electron with the redox center located inside the protein (eq 3a). Addition of a sacrificial donor (D = aniline or EDTA) reduces the surface-bound Ru^{3+} complex (eq 3b), so that the net effect of photoexcitation is rapid generation of the reduced state of the redox protein. Photoexcitation in the presence of the partner protein (M^+) leads to interprotein ET (eq 3c).

$$(*Ru^{2+}-Fe^{3+}) \rightarrow (Ru^{3+}-Fe^{2+}) \quad (3a)$$

$$(Ru^{3+}-Fe^{2+}) + D \rightarrow (Ru^{2+}-Fe^{2+}) \quad (3b)$$

$$(Ru^{2+}-Fe^{2+}) + M^+ \rightarrow (Ru^{2+}-Fe^{3+}) + M \quad (3c)$$

This approach has the advantage, not yet realized in experiment, that it can be used to study any protein pair, including those in which *neither* partner contains a heme. However, the presence of the Ru complex can strongly perturb the delicate balance of interactions that govern complex formation; the required attachment of a large and often highly charged group must have a profound effect on the strength and even the mode of protein−protein binding. In short, the heme replacement and "redox-attachment" techniques are substantially complementary to each other.

III. Multisite and Multidomain Binding: Microscopic vs Thermodynamic Constants

When two proteins act as ET partners, the first level of inquiry is to establish the stoichiometry of the reaction and to identify the domain or domains where binding occurs. The second, experimentally correlated question is whether binding at a particular domain involves multiple conformations and whether interconversion among domains and/or sites within them influences or even gates the ET process. Here we define binding "domains" as nonoverlapping surface regions that can bind substrates simultaneously; a domain may exhibit one or more overlapping "sites" that cannot be occupied simultaneously. The kinetics of complex formation and dissociation, as well as those of conformational interconversion, can control the experimental observations and are phenomena of primary interest in their own right. However, they also must be understood before the ET event itself can be characterized. As we now discuss, in general one does not measure the microscopic affinity or reactivity constants for an individual domain or site, but rather so-called thermodynamic or stoichiometric constants that are fewer in number than the microscopic constants. Such distinctions and their consequences are well-known in studies of ligand binding to proteins and receptors[35−37] but have not been appreciated in the study of protein−protein ET complexes.

A. 1:1 Stoichiometry

The simplest case of 1:1 binding of one protein (the "substrate", S) by a second protein ("enzyme", E) is described by eq 4:

$$E + S \rightleftharpoons ES \quad (4)$$

$$K_1 = \frac{[ES]}{[E][S]}$$

Taking the "enzyme" as the probe (denoted by a "dagger"), the fraction (*f*) of binding sites on $E^\dagger$ that are occupied with an S molecule is obtained by solving the thermodynamic equation for binding (eq 4). It is common practice to determine the binding equilibrium constant (K_1) and intraprotein ET rate constant (k_1) through kinetic measurements of the

intracomplex ET rate constant during the course of a titration of one component by the other.[38,39] In the classical Stern−Volmer[40] procedure this determination would involve a quenching titration of a photoactive "probe" by its partner as the quencher. However, to analyze the results it is necessary to consider the dynamics for the equilibrium exchange between bound and free species. The decay traces in a quenching titration are determined by both the intracomplex quenching rate constant (k_1) and the rate constants for the formation and dissociation of the complex (k_{on} and k_{off} where $K_1 = k_{on}/k_{off}$). In the rapid-exchange limit where $k_{off} \gg k_1$, the experimental decay traces are exponential. The measured quenching rate constant (Δk) at any point in a titration, given by eq 5, increases monotonically with

$$\Delta k = k_1 \frac{[E^\dagger S]}{[E^\dagger]_0} \equiv k_1 f \qquad (5)$$

the weighted average population of the bound state ($f = [E^\dagger S]/[E^\dagger]_0$, where $[E^\dagger]_0$ is the total concentration of E). In the slow-exchange limit where $k_{off} \ll k_1$, the decay traces are biexponential with rate constants that correspond to the lifetimes of the free and bound states. In this case, the observed rate constants are invariant with concentration, and instead, the fractional weight of the faster of the two kinetic phases equals f. With intermediate exchange rate constants, detailed analysis of the process curves is required to determine the affinity constant and the microscopic reactivity constant. Thus, a measurement of the binding equilibrium necessarily yields information about the interconversion dynamics for binding.

At the next level of complexity, one protein (E) may bind another (S) with a 1:1 stoichiometry, but the binding domain on the surface of E may have multiple, overlapping (exclusive) binding sites. An alternate way to describe this is that there are multiple binding conformations of ES. If there are n sites and thus n conformers of the 1:1 complex (^{1}ES, ^{2}ES, ..., ^{n}ES), each configuration can be assigned its own binding constant (K_{10}, $K_{20,}$, ... K_{n0}) and its own reactivity constant ($^1k_1$, $^2k_1$, ... $^nk_1$). In such a case, the kinetics of the observed ET process can be altered or even controlled ("gated") by conformational interconversion, rather than by the ET event.[15,41]

To explore the consequences of coupling ET to conformational dynamics, we considered the simplest model for any gated reaction, a donor−acceptor pair, [E†,S], where E† is the photodonor and each of the three system states involved in the photoinitiated ET cycle described in eqs 1 and 2 (ES, E†S, and I) exhibits two conformational substates (ES = ^{1}ES + ^{2}ES, E†S = ^{1}E†S + ^{2}E† S, and I = ^{1}I + ^{2}I).[15] Within the present context, such a reactive pair could also represent a complex in the slow-exchange limit. The introduction of conformational interconversion expands the simple bound-state ET mechanism of eqs 1 and 2 to Scheme III.1. This scheme includes ET rate constants only for the E†S → I ET processes in which the system conformation is conserved so that conformational and ET steps only occur sequentially. Intuitively, it might be expected that the kinetic scheme must include ET that is synchronous with a conformational change in the medium coordinate. However, we

Scheme III.1

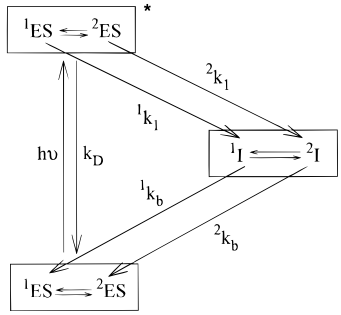

showed that, for all practical purposes, it is not necessary to include the "diagonal" processes (e.g., ^{1}E†S → ^{2}I) when considering stable substates, only the "square scheme" shown.

The complete solutions for the concentrations of E†S(t) and I(t) for Scheme III.1 have been presented,[15,41] and in general one expects to observe complex, multiexponential behavior. However, in two limiting cases the functional forms for both E†S(t) and I(t) will reduce to those predicted by the simple cycle of eqs 1 and 2 for a complex with only a single conformation. Thus, the direct kinetic observations give no evidence of the existence of multiple conformations. However, the measured rate constants are not those for an ET event. In one extreme, the "gating" limit, the intrinsic ET rate constants are much faster than the conformational interconversions, which thus become rate limiting. Because standard detection methods monitor only the ET event and do not reflect the identity of the conformer involved, in many, if not most, instances the measurements of the time course of an ET reaction are themselves unlikely to distinguish whether or not the reaction is gated. Fortunately, the partial decoupling of the ET and conformational processes afforded by the absence of synchronous events, in principle and in practice, allows for the identification of an observed decay rate constant with a microscopic rate constant.

Of critical importance to this discussion is a second limiting case where the conformational substates interconvert rapidly compared with the ET rate constants. Again, the kinetics are indistinguishable from those for a single conformation. In particular, when there are two rapidly interconverting conformations (two binding sites within a domain), the measurements can be described with a single stoichiometric affinity constant (K_A) which is related to the microscopic site affinity constants through eq 6.

$$K_A = K_{10} + K_{20} \qquad (6)$$

When exchange between the bound complexes and their free components is rapid, the observed quenching rate constant at any point in a titration (Δk) is a weighted average of the two site rate constants, where the weighting is given by the fractional populations of photodonor incorporated in the individual conformers according to eq 7.

$$\Delta k = {}^1k_1 \frac{[{}^1E^\dagger S]}{[E^\dagger]_0} + {}^2k_1 \frac{[{}^2E^\dagger S]}{[E^\dagger]_0} \qquad (7)$$

This can be rewritten in terms of a single stoichio-

Scheme III.2

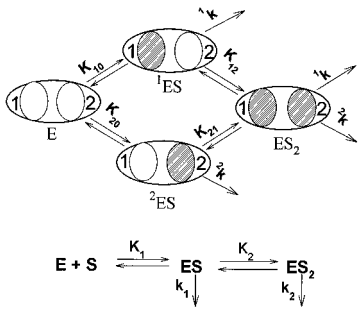

metric rate constant (k_A) and the fractional population of $E^{\dagger}S$, f (defined in eq 5).

$$\Delta k = \left({}^1k_1\frac{K_{10}}{K_A} + {}^2k_1\frac{K_{20}}{K_A}\right)\frac{[E^{\dagger}S]}{[E^{\dagger}]_0} \tag{8}$$

$$\equiv ({}^1k_1\,{}^1g_1 + {}^2k_1\,{}^2g_1)f \equiv k_A f$$

The stoichiometric rate constant (k_A) is a weighted average of the individual site rate constants ($^1k_1$ and $^2k_1$), where the weighting factor, $^ig_1$, is the fraction of 1:1 complex where S is bound at site i. Extension of this idea to the case where there are n exclusive binding sites within a single domain shows that the stoichiometric binding constant is the sum of the individual site binding constants and the stoichiometric rate constant is a weighted sum of all the individual site rate constants (eq 9).

$$K_A = \sum^{i} K_{i0} \tag{9}$$

$$k_A = \sum^{i} {}^ik_1\frac{K_{i0}}{K_A} = \sum^{i} {}^ik_1\,{}^ig_1$$

Note that eq 8 is identical in form to eq 5 for simple 1:1 binding. Thus, whereas $2n$ microscopic constants are required to describe the n-site case ($^ik_1$, K_{i0} for each), measurements, such as quenching, that are not site-specific give only the two stoichiometric parameters (K_A and k_A), both of which represent configuration averages.

B. 2:1 Stoichiometry

To illustrate the extension of these ideas to stoichiometries greater than 1:1, consider an enzyme ($E^{\dagger}$) that simultaneously binds two molecules of a substrate (S) at distinct and *nonexclusive* domains. When the two domains exhibit nonidentical affinities, there are two 1:1 complexes, one having the high-affinity domain occupied (^{1}ES) and the other having the low-affinity domain occupied (^{2}ES), giving four possible states for the ES_2 system (Scheme III.2). As illustrated, there are two alternative pathways for proceeding from free donor ($E^{\dagger}$) to the fully saturated ES_2 complex, and these differ in the order in which the two independent domains become occupied. If the affinity, but not the reactivity, of a given domain changes when other domains are occupied, there are six domain constants (^1k, ^2k, K_{10}, K_{20}, K_{12}, and K_{21}). In the most general case where the domain rate constants depend on the occupancy of the other domains, there would be eight domain parameters.

However, when binding studies do not probe the properties of the individual domains, only the stoichiometric binding constants (K_1 and K_2) associated with eq 10 can be measured.

$$E + S \overset{K_1}{\rightleftharpoons} E + S \tag{10}$$

$$ES + S \overset{K_2}{\rightleftharpoons} ES_2$$

Moreover, under the common condition of rapid exchange only the stoichiometric rate constants (k_1 and k_2) can be measured for the 1:1 and 2:1 species, respectively. We discuss binding constants first. The relationships between the stoichiometric binding constants and the domain binding constants in Scheme III.2 are given by eqs 11 and 12.

$$K_1 = K_{10} + K_{20} \tag{11}$$

$$K_1K_2 = K_{10}K_{12} = K_{20}K_{21} \tag{12}$$

Here K_{i0} (i = 1,2) are the domain binding constants for binding S at domain i of E; K_{12} and K_{21} are the domain binding constants for binding a second molecule of S to the vacant domain of ES, where the subscripts indicate the order in which the two domains become occupied.

Turning to rate constants, when the rapid-exchange limit holds for a system with 2:1 binding, the observed quenching (Δk) depends on the fraction of the total concentration $E^{\dagger}_0$ that is incorporated into $E^{\dagger}S$ and $E^{\dagger}S_2$ (f_1 and f_2) and the rate constants associated with the two stoichiometric binding stages (k_1 and k_2) (eq 13).

$$\Delta k = k_1\frac{[E^{\dagger}S]}{[E^{\dagger}]_0} + k_2\frac{[E^{\dagger}S_2]}{[E^{\dagger}]_0} = k_1f_1 + k_2f_2 \tag{13}$$

If one assumes that the reactivity of a given domain is independent of the occupancy of all other domains (thereby ignoring the possibility of "reactivity cooperativity"), the stoichiometric rate constants (k_1 and k_2) of eq 13 are functions of the rate constants that describe ET at an individual domain (^1k and ^2k; see Scheme III.2) as given by eqs 14 and 15

$$k_1 = {}^1k\frac{K_{10}}{K_1} + {}^2k\frac{K_{20}}{K_1} = {}^1k\,{}^1g_1 + {}^2k\,{}^2g_1 \tag{14}$$

$$k_2 = {}^1k + {}^2k \tag{15}$$

where the weighting factor $^ig_1$ is the fraction of $E^{\dagger}$ that is incorporated in a 1:1 complex in which S is bound to domain i, as in eq 8. Thus, binding at two domains in the rapid-exchange limit is described by four stoichiometric constants (K_1, K_2; k_1, k_2) but by six domain constants (Scheme III.2). The thermodynamic relationships between domain binding constants expressed in eqs 11, 12, 14, and 15 supply an

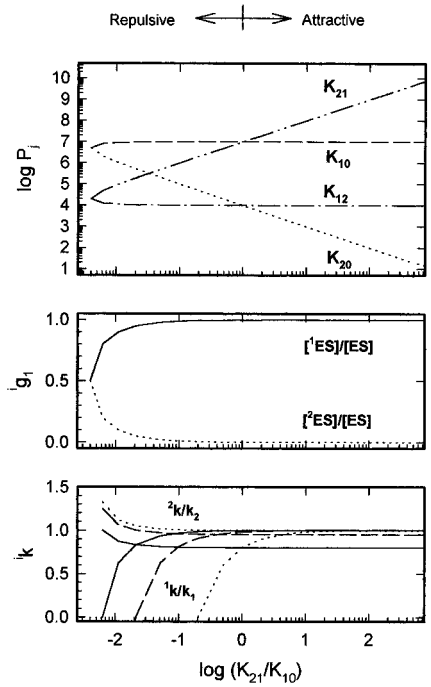

Figure III.1. Combinations of the domain affinity constants (upper), derived distribution functions (middle), and domain rate constants (lower) that are compatible with the stoichiometric constants $K_1 = 10^7$ M^{-1} and $K_2 = 10^4$ M^{-1}, as a function of the relative attractive (or repulsive) interaction between the two domains. Lower panel: Derived site rate constants (^1k and ^2k) for $k_2/k_1 = 5$ (−), 20 (- -), and 200 (···) with $k_1 = 100$ s^{-1}.

additional constraint, so there are five independent domain constants.

A unique solution for all five independent domain constants obviously cannot be obtained from the four measured stoichiometric constants. If one treats one domain constant as a parameter, then the combinations of domain constants that are compatible with a given set of stoichiometric constants can be calculated using eqs 11, 12, 14, and 15. The upper panel of Figure III.1 illustrates the combinations of domain affinity constants that are allowed for stoichiometric constants of $K_1 = 10^7$ M^{-1} and $K_2 = 10^4$ M^{-1}; the independent parameter is chosen to be K_{21}/K_{10}, which is a measure of the interactions between molecules bound at the two domains. Thus, if $K_{21}/K_{10} > 1$, it is easier to bind a molecule of S at one domain when the other domain is already occupied (attractive interaction); if $K_{21}/K_{10} < 1$, then molecules bound at the two domains repel each other. For noninteracting molecules, $K_{21}/K_{10} = 1$.

The middle panel of Figure III.1 presents the derived distribution functions, $^1g_1$ and $^2g_1$, given by eq 14 as a function of K_{21}/K_{10}. When the domains are noninteracting, binding at the high-affinity domain dominates so that [^{1}ES] > [^{2}ES]. As K_{21}/K_{10} is decreased (which corresponds to increasing repulsion between molecules bound at the two domains), the weighting factor for ^{2}ES increases while that for ^{1}ES decreases. Thus, for fixed domain constants, one sees that repulsive interdomain interactions tend to equalize the populations of ^{1}ES and ^{2}ES. On the other hand, attraction between molecules bound at the two domains ($K_{21} > K_{10}$ in Figure III.1) accentuates the dominance of the high-affinity domain, so that the relative populations of ^{1}ES and ^{2}ES approaches the ratio of the stoichiometric affinity constants ([^{1}ES]/[^{2}ES] = K_1/K_2).

The lower panel of Figure III.1 presents the values of the relative site reactivity constants ($^1k/k_1$ and $^2k/k_2$) as a function of K_{21}/K_{10}, derived for several assumed relative stoichiometric reactivities. For a given set of stoichiometric parameters, $^1k/k_1$ decreases toward a lower bound of zero and $^2k/k_2$ increases, as repulsion between the two domains becomes more significant. As the difference between the reactivity constants (k_2/k_1) becomes large, the value of K_{21}/K_{10}, for which $^1k \rightarrow 0$, increases, indicating that the degree to which repulsions can be significant diminishes.

The relationships between domain affinity constants and stoichiometric affinity constants summarized in eqs 11, 12, 14, and 15 are useful when interpreting changes in the apparent stoichiometry and/or affinity that are induced either by a perturbation in the solution conditions or by an alteration of the complex itself through site-directed mutagenesis and/or chemical modification (see section VI). When binding at one domain is weakened, eqs 11 and 12 require that the change in one domain binding constant necessarily is accompanied by a change in the other. For example, a mutation that weakens binding at one domain will necessarily reduce both K_1 and K_2. Because the formation of a ternary complex requires two consecutive steps—one with weakened binding followed by a second step involving even weaker binding—the amount of 2:1 complex could become quite small.

Likewise, such relationships between the stoichiometric constants and the domain constants provide the means for analyzing the dependence of ET rate constants on state variables (temperature, pressure, ionic strength, etc.) in terms of changes in the distribution among multiple forms of a complex. If the domain binding constants change differentially with a state variable, the relative populations of the multiple conformers could shift, so that, according to eq 14, a measured stoichiometric rate constant could change even without changes in the domain rate constants.

IV. Quenching as a "4-D" Experiment

In the "normal" (N) excited-state titration protocol that originated with Stern and Volmer[40] almost three-quarters of a century ago, aliquots of the quencher molecule are added into a solution containing a fixed concentration of the luminescent probe molecule, and the resulting plot of quenching (Δk) versus titrant is fit to a mechanism. (For convenience, we discuss rapid-exchange situations in this section; slow exchange can be treated similarly.) Thinking of the quenching experiment in terms of such curves hides the fact that the measured quenching rate constant is, in fact, a function of both the probe and the quencher concentrations, and the values of this function can be represented by a two-dimensional surface. The goal of characterizing the binding between E and S and the reactivity of the complex (or complexes) they form thus can be translated into a goal of determining the shape of the 2-D Δk surface.

Table IV.1. Titration Protocols for ES_2 Complexes

	conventional substitution		inverse substitution	
titration	$E^\dagger$	S	E	$S^\dagger$
C_N		titrant		
C_R	titrant			
I_N			titrant	
I_R				titrant

This perspective opens avenues of approach that greatly enrich the productivity of quenching experiments. For example, the simplest case of 1:1 binding is symmetric in that it makes no difference which partner contains the luminescent probe. (In this review E (or S) becomes the probe primarily through heme replacement, although other types of experiments are possible.) However, if it is known or suspected that higher stoichiometries may be involved, say if E binds two S molecules, then the results are *not* symmetric. We denote as a conventional (C) experiment one in which E is the probe molecule; we denote the experiment where the probe is S as an inverse (I) experiment. In either case, a N titration, in which the quencher is the titrant, generates a slice through the Δk surface that is parallel to the quencher axis (see Figures IV.2, IV.5, and IV.8). As we show below, and perhaps surprisingly, it is advantageous to use a new type of experiment, a "reverse" (R) titration, in which titrating the probe into a solution containing a fixed concentration of the quencher generates a slice through the Δk surface that is parallel to the probe axis. With each of the two options for metal substitution, C and I, titrations can be performed in the normal way (N) or the reverse way (R). Thus, the results of a traditional Stern−Volmer quenching experiment of the past are, in fact, best thought of as one subset of a 4-D dataset generated from four distinct types of titrations: C_N, C_R, I_N, and I_R (Table IV.1).

A. Conventional Titrations (C_N and C_R) with 1:1 Stoichiometry

Consider a representative Δk surface for moderately strong 1:1 binding of S to E ($K_1 = 10^5$ M^{-1}), as indicated in Figure IV.1, where we have arbitrarily chosen S as the quencher and $E^\dagger$ as the probe. The N titration, in which quencher (S) is progressively added to a solution containing the probe ($E^\dagger$) at fixed

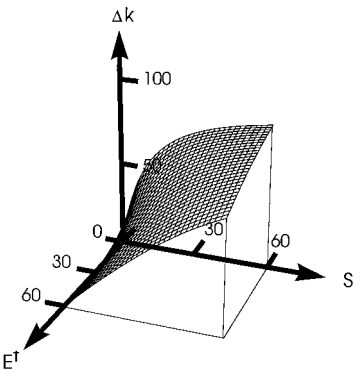

Figure IV.1. Surface plot describing quenching (Δk) within an $E^\dagger S$ complex as a function of the concentrations of substrate (S) and enzyme ($E^\dagger$). Simulation parameters: $K = 10^5$ M^{-1} and $k = 100$ s^{-1}.

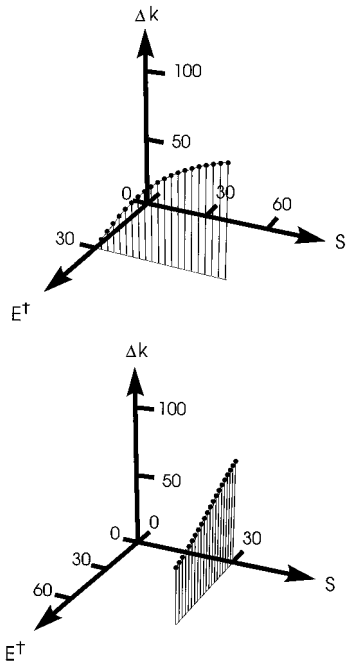

Figure IV.2. Slices through the 1:1 binding surface of Figure IV.1 showing a normal (N) Stern−Volmer titration (upper panel) and a reverse (R) Stern−Volmer quenching experiment (lower panel).

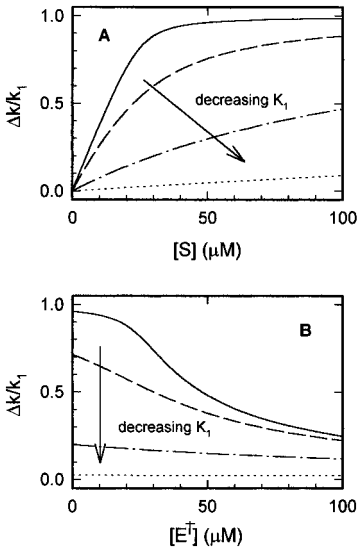

Figure IV.3. Plot of $\Delta k/k_1$ for titrations simulated for a range of K_1: Upper panel, N-titration, $[E]_0 = 25$ μM; Lower panel, R-titration, $[S]_0 = 25$ μM. Simulation parameters: (—) $K = 10^6$ M^{-1}, (– – –) $K = 10^5$ M^{-1}, (–·–) $K = 10^4$ M^{-1}, (···) $K = 10^3$ M^{-1}.

concentration (Figure IV.2) corresponds to a slice through the Δk surface that is parallel to the quencher axis and has an intercept of $\Delta k_0 = 0$ when [S] approaches zero. The binding and kinetic parameters that describe quenching for 1:1 stoichiometry (K_1 and k_1) are derived from the hyperbolic shape of the Δk titration curve. As binding gets weaker, however, it becomes increasingly more difficult to accurately determine the curvature of the quenching curve, and finally one reaches a limit where only a straight line, the slope of which gives the product $M = K_1 k_1$, is observable (Figure IV.3, upper).

By representing Δk as a surface, it is obvious that there is an alternate "reverse" titration experiment (R) in which titration with the probe generates a slice

through the Δk surface that is parallel to the probe axis. At first thought this may appear useless, because there is nothing to measure in the early phases of such a titration! However, modern instrumentation is so sensitive that it is trivial to perform measurements with extremely low concentrations of the probe, and we find that the intercept as $[E^{\dagger}] \rightarrow 0$ (Δk_0) can be measured quite reliably. Once this is recognized, a look at the Δk surface shows that the normal and reverse experiments are not symmetry-equivalent, even for the assumed 1:1 stoichiometry. The reason for this lies in the recognition that reverse titrations necessarily give well-defined, *nonzero* values for Δk_0, whereas the intercept in a normal quenching experiment is zero. For a 1:1 binding model, Δk_0 for a reverse titration is given by eq 16:

$$\Delta k_0 = \frac{k_1 K_1 [S]_0}{1 + K_1 [S]_0} \tag{16}$$

A key advantage to a reverse titration is that this expression provides a further constraint on the relationship between the desired fitting parameters. The intercept can be used to eliminate either K_1 or k_1, thereby reducing the number of independent fitting parameters and greatly enhancing the reliability of an analysis of experimental data.

Just as the characteristics of a traditional titration change progressively from linear in the limit of weak binding to hyperbolic in the limit of strong binding, the shape of a reverse titration varies characteristically as K_1 decreases. Figure IV.3 (lower) shows a set of simulated reverse titrations for 1:1 stoichiometry with $10^3\ M^{-1} < K_1 < 10^6\ M^{-1}$. For strong binding, Δk remains roughly constant during a reverse titration until a concentration ratio of ~1:1, and then it decreases rapidly with subsequent additions of the probe. If K_1 has an intermediate value, then Δk decreases smoothly and monotonically during a reverse titration. For the initial stages of the titration, the decrease in Δk is linear with increasing S, and by combining the measured values for the initial slope and for Δk_0, one can obtain extremely well-defined values for both K_1 and k_1. Finally for very weak binding, Δk is nearly invariant, even up to rather high concentrations of the probe, and the initial slope can no longer be reliably measured. In this case, the product $K_1 k_1$ can be determined from the intercept, but the individual parameters (K_1 and k_1) cannot be independently determined with either a normal titration or a reverse titration. Thus, the same limitations ultimately apply to both the traditional C_N titration experiment and the new C_R titration. However, in practice, it appears that one can more often and more reliably determine the individual parameters K_1 and k_1 with the *R* protocol.

Even better than relying on but one type of experiment is to combine them. The simultaneous analysis of data from a normal titration and a reverse titration provides an alternative method for independently determining K_1 and k_1. The initial slope obtained from a normal titration ($M = K_1 k_1$) and the intercept obtained from a reverse titration (Δk_0), where the concentration of S is fixed as $[S]_0$ can be combined to calculate K_1

$$K_1 = \frac{M}{\Delta k_0} - \frac{1}{[S]_0} \tag{17}$$

and this parameter then can be used with M to calculate k_1.

B. Conventional (C) Titrations with 2:1 Stoichiometry

The introduction of a broadened perspective is most beneficial when stoichiometries other than 1:1 are known or suspected to occur. In the present section we focus on the case where E can bind up to two molecules of S. Figure IV.4 shows the surfaces that describe the fractions of probe $E^{\dagger}$ that are incorporated into the 1:1 and 2:1 complexes as a function of the two independent variables ($[E^{\dagger}]$ and [S]) for a conventional titration where the *stoichiometric* binding constants are $K_1 = 10^7\ M^{-1}$ and $K_2 = 10^4\ M^{-1}$. Clearly the shapes of the 1:1 and 2:1 surfaces differ greatly, and the proper choice of titration protocol can take advantage of this.

C_N Titration

When kinetic measurements are used to probe binding affinity and stoichiometry, the observed quenching constant is a weighted average of the stoichiometric quenching constants for the 1:1 and

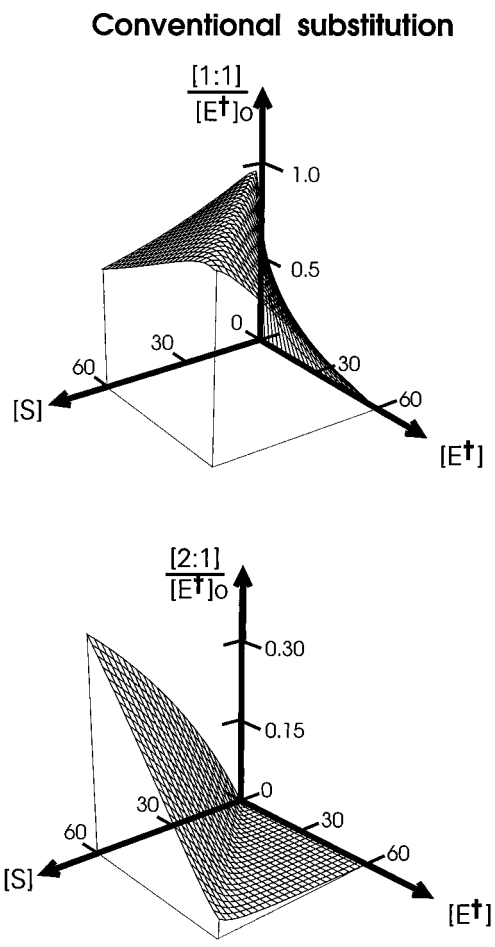

Figure IV.4. Surfaces for the conventional (C) substitution mode describing the fractions of $E^{\dagger}$ that are incorporated into the $E^{\dagger}S$ (1:1) and $E^{\dagger}S_2$ (2:1) complexes as a function of the concentrations of substrate (S) and enzyme ($E^{\dagger}$). Simulation parameters: $K_1 = 10^7\ M^{-1}$, $K_2 = 10^4\ M^{-1}$.

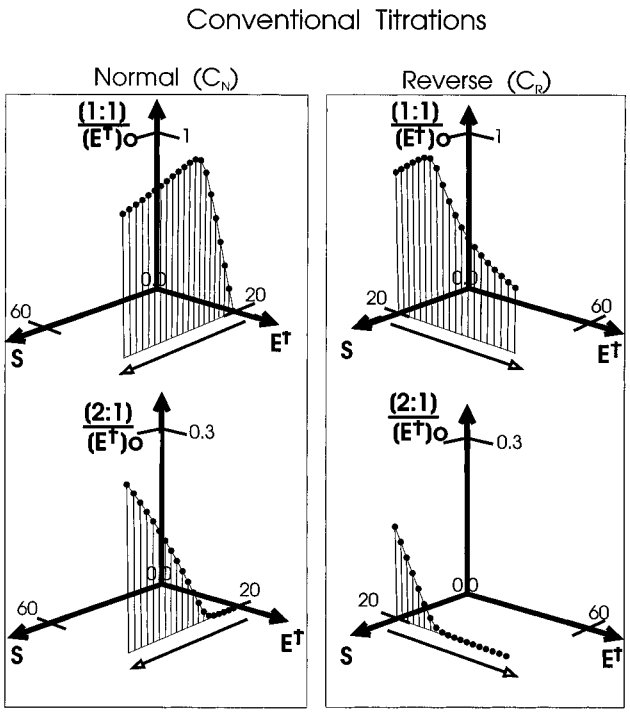

Figure IV.5. Slices through the two-dimensional surfaces of Figure IV.4 describing the fractions of $E^{\dagger}$ that are incorporated into the 1:1 and 2:1 complexes for the conventional (C) substitution protocol: left panel, C_N titration; right panel, C_R titration.

2:1 complexes, with the weighting corresponding to the fractional populations of these species (eqs 14 and 15). For the conventional (C) metal substitution mode, titration curves generated by the C_N protocol, where $E^{\dagger}$ is the luminescent probe and the quencher (S) is the titrant, sequentially reflect the two stages of binding; the 1:1 complex predominates in the initial stage of the titration, and subsequent additions of quencher ultimately convert the 1:1 complex to the 2:1 complex (Figure IV.5, left panel). Regardless of the *domain* reactivities, the *stoichiometric* rate constant for the second stage of binding (k_2) is necessarily larger than that for the first stage of binding (eqs 14 and 15). Thus, Δk monotonically increases with progressive addition of quencher ($E^{\dagger}$) *regardless* of the binding stoichiometry.

Any attempt to differentiate between 1:1 binding and 2:1 binding is only favorable when both the stoichiometric affinity constants and the stoichiometric reactivities differ appreciably for the two binding stages. If the two stages of binding are not well-separated either because the affinities for the two stages are similar or because their reactivities are too similar, then the experiment is unreliable for establishing the binding stoichiometry and certainly provides no reliable determination of the parameters for the second binding step. If one domain is much more reactive and dominates the observed quenching, (i.e., if either ^1k or ^2k is much larger than the other), then the two binding steps can be clearly resolved and the Δk surface will track that of the dominant species.

When binding is monitored by measuring proton uptake (or release) or by binding-induced changes in chemical shift for an NMR experiment, the properties of the two domains may differ in both magnitude and sign (section VI.E). In such studies, there are

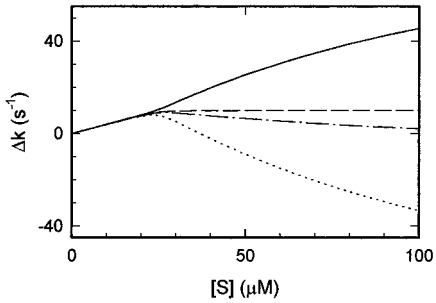

Figure IV.6. Effect of the relative magnitude and sign of the reactivity parameters (k_1, k_2) on the C_N titration curves (eq 13). Simulation parameters: $[E^{\dagger}] = 25\ \mu M$; $K_1 = 10^7\ M^{-1}$, $K_2 = 10^4\ M^{-1}$, $k_1 = 10\ s^{-1}$; (—) $k_2 = 100\ s^{-1}$, (– – –) $k_2 = 10\ s^{-1}$, (–·–) $k_2 = -10\ s^{-1}$, (···) $k_2 = -100\ s^{-1}$.

"reactivity" parameters analogous to k_1 and k_2 that describe the properties of the individual binding steps, and when both the magnitudes and signs differ for the two stages of binding, the titration curves can have unusual shapes that unambiguously signal the presence of 2:1 binding (or higher). Figure IV.6 shows a series of C_N titration curves where the stoichiometric affinities are fixed ($K_1 = 10^7\ M^{-1}$ and $K_2 = 10^4\ M^{-1}$) but the relative stoichiometric reactivities are varied in both magnitude and sign. In the case where $k_2/k_1 > 10$, the titration curve shows two phases and the observed reactivity increases monotonically. When the stoichiometric reactivities for the two binding stages also differ in sign, the measured reactivity (Δk) no longer increases monotonically but instead exhibits a maximum at $R \approx [S]/[E] = 1$. Even though it is not possible to differentiate two binding steps when the stoichiometric reactivities have equal magnitude and sign, they can be resolved readily when the two stages of binding exhibit identical reactivities of *opposite* sign.

C_R Titration

When $E^{\dagger}$ is the probe, the two binding steps may well be more readily resolved with a reverse titration (C_R), in which $E^{\dagger}$ is titrated into a solution containing a fixed concentration of S. The right panel of Figure IV.5 shows a slice through the 2-D surfaces for the fractional populations of the 1:1 and 2:1 complexes during such a C_R titration. As $[E^{\dagger}]$ increases, the population of the 2:1 complex decreases monotonically, while the population of the 1:1 complex increases slightly until $R = [E^{\dagger}]/[S] = 1$, then decreases sharply. In general, one can differentiate between 1:1 binding and 2:1 binding by the shape of a C_R curve. Thus, for 2:1 binding when k_2 is sufficiently much greater than k_1 (recall from above that necessarily $k_2 > k_1$), Δk exhibits a sharp decrease well before $[E^{\dagger}] = [S]$, but as discussed above, for tight 1:1 binding Δk decreases gradually only after $[E^{\dagger}] > [S]$. Inspection of Figure IV.5 shows that the decrease in Δk beyond $R \sim 1/2$ for the 2:1 case occurs because further additions of $E^{\dagger}$ convert the more reactive ternary complex to the less reactive binary complex.

For 2:1 binding, as for 1:1 binding, the quenching constant in a C_R titration has a nonzero intercept as $[E^{\dagger}] \rightarrow 0$, with Δk_0 for the 2:1 case given by eq 18

$$\Delta k_0 = \frac{k_1K_1[S]_0 + k_2K_2[S]_0^2}{1 + K_1[S]_0 + K_1K_2[S]_0^2} \qquad (18)$$

where $[S]_0$ again is the initial concentration of the quencher. The first term is the contribution to Δk_0 arising from the 1:1 complex and the second term gives the contribution due to the ternary complex. Again, the extrapolated value for Δk_0 can be used to replace one of the four stoichiometric fitting parameters. When K_1 is large, Δk_0 is least sensitive to this parameter, so one would normally eliminate K_1. If the values of K_1 and k_1 can be obtained from a C_N experiment, then one could also fix these parameters and instead eliminate one of the two parameters characterizing the second binding step.

C. Inverse Titrations (I_N and I_R)

When complex formation involves a ternary ES_2 complex, the experiments are no longer symmetric with respect to metal substitution; quenching measurements for C substitution, where the luminophore is in E, and for I substitution, where the luminophore is in S, yield complementary, *not* identical, results. The characteristics of the two types of titrations, N and R, for the I substitution mode ($S^\dagger$ as probe) are illustrated in 2-D surfaces plots describing the fractions of $S^\dagger$ that are incorporated in the 1:1 and 2:1 complexes (Figure IV.7) for a system that employs the same stoichiometric binding constants used in Figure IV.4. These surfaces have complex shapes.

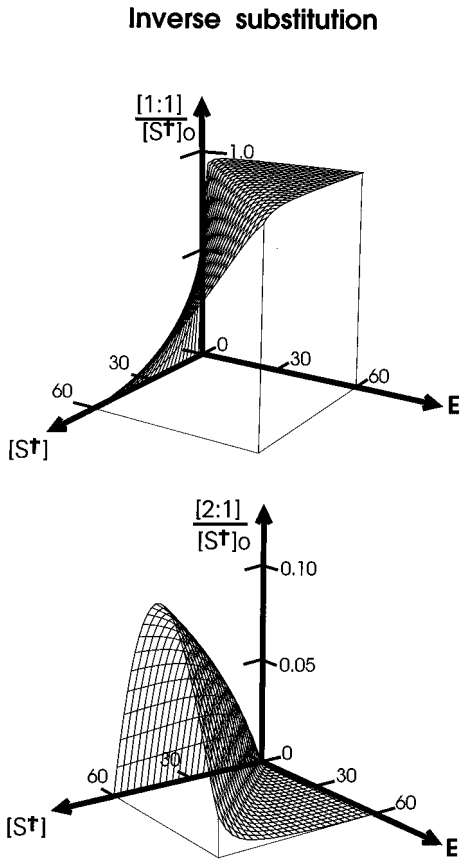

Figure IV.7. Surfaces for the inverse (I) substitution mode describing the fractions of $S^\dagger$ that are incorporated into the ES (1:1) and ES_2 (2:1) complexes as a function of the concentrations of substrate ($S^\dagger$) and enzyme (E). Simulation parameters: Same as for Figure IV.4.

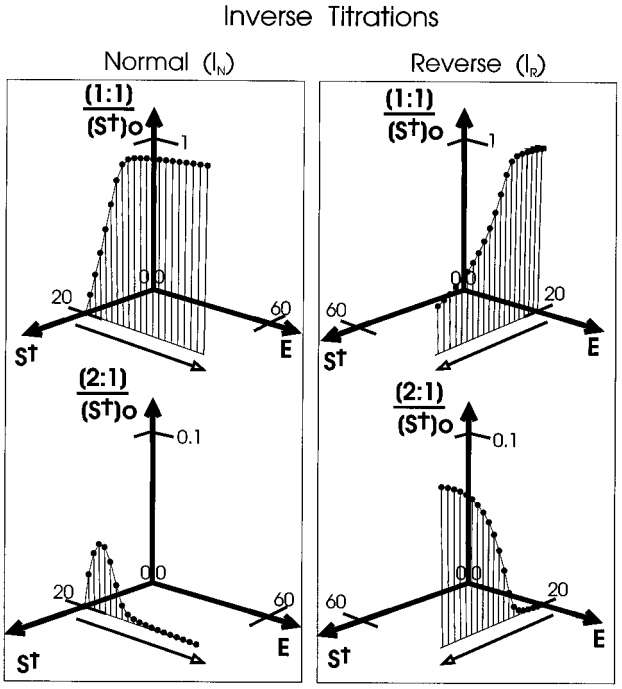

Figure IV.8. Slices through the two-dimensional surfaces of Figure IV.7 describing the fractions of $S^\dagger$ that are incorporated into the 1:1 and 2:1 complexes for the inverse substitution protocol: left panel, I_N titration; right panel, I_R titration.

In particular, the surface for the 2:1 complex is striking in that it shows local maxima in regions away from the axes. As a result, experiments with I substitution permit for a better determination of binding and kinetic parameters.

I_N Titration

Consider first a slice parallel to the E-axis, generated by an I_N titration of $S^\dagger$ by the quencher, E (Figure IV.8, left panel). During such an I_N titration, the population of 1:1 complex increases monotonically, while the population of ES_2 increases from zero at $[E] = 0$ to a maximum at $R = [E]/[S^\dagger] = {}^1/_2$, then decreases toward zero as [E] increases. As discussed above, if the stoichiometry of binding is 1:1, then Δk necessarily increases monotonically with addition of E. However, for 2:1 binding this need not be so. In a system where quenching is dominated by the reactivity of the 2:1 complex, Δk would be essentially proportional to $f_2 = [ES^\dagger_2]/[S^\dagger]_0$ and the I_N quenching curve would show a maximum near $R = [S^\dagger]/[E] = 2$. The observation of such nonmonotonic changes in Δk would *require* a stoichiometry of 2:1 (or greater) (see section VI).

I_R Titration

Now consider a slice parallel to the $S^\dagger$-axis generated by an I_R titration (E titrated by $S^\dagger$); the fractional populations of the 1:1 and 2:1 complexes are shown in Figure IV.8, right panel. Once again there will be a nonzero intercept (Δk_0), with the applicable expression being that of eq 16, but with $[S]_0$ replaced by $[E]_0$. The concentration of the ternary complex is low in the limit where $[S^\dagger] \rightarrow 0$, and consequently, the initial phase of the titration curve tracks the reactivity of the 1:1 complex; subsequent additions of S convert the 1:1 complex to the 2:1 complex, but

the fractions of 1:1 and 2:1 complex are roughly constant as the concentration of $S^{\dagger}$ increases toward $[S^{\dagger}] \sim [E]$. Additions of $S^{\dagger}$ beyond the $R = 1$ point would necessarily cause Δk to decrease if there is tight 1:1 binding. However, when the stoichiometry is 2:1, Δk can increase during the titration, if the ternary complex exhibits appreciable quenching (k_2 is large), and the result would be a maximum in Δk during a titration. The observation of such behavior also would *require* 2:1 stoichiometry (or greater).

In summary, one can use either E (conventional substitution) or S (inverse substitution) as the probe, and whenever possible one should use both. Each experiment is best understood in terms of its own 2-D surface plot, and each experiment can be performed in either the normal (N) way, where aliquots of the quencher are added into a solution containing a fixed concentration of the probe, or the reverse (R) way, where aliquots of the probe are titrated into a solution in which the concentration of the quencher is fixed. Although we have emphasized how these new titration experiments can be applied to analyze the kinetic data from a series of flash photolysis experiments, these new titration experiments could, and indeed should, be used when designing and analyzing titration experiments in which other properties are monitored. As is shown in section VI for the complex between C*c*P and C*c*, the characteristic shapes of the inverse and reverse titration curves provide a far clearer distinction between 1:1 and 2:1 stoichiometry than a traditional titration, but it is through combinations of these experiments that a definitive determination of stoichiometry and reactivity can best be achieved.

V. Unimolecular and Bimolecular Electron Transfer in Biomolecules

In a single fixed donor (D)−acceptor (A) geometry, the ET reaction rate is well defined. In long range ET systems, the donor and acceptor are weakly coupled (electronically) by the intervening protein, and the rate is nonadiabatic and is proportional to the square of the protein-mediated donor−acceptor coupling multiplied by a nuclear Franck−Condon factor (FC) (eq 19).[9,42]

$$k_{ET} = \frac{2\pi}{\hbar} T_{DA}{}^{2} FC \qquad (19)$$

FC reflects the thermal density of states for resonant donor and acceptor levels. In the equilibrium molecular geometry, these donor and acceptor electronic levels are not necessarily of equal energy, so the process can be activated. By discussing the Franck−Condon factor in terms of density of states, the rate can be thought of in the context of Fermi's golden rule with thermal averaging over the initial state distribution.[42] The tunneling matrix element, T_{DA}, reflects the bridge-mediated coupling between donor and acceptor states at the resonant configuration(s). The tunneling matrix element is controlled not only by the chemistry and energetics of donor and acceptor but also by the protein bridge that links them and couples them electronically. The unimolecular rate is influenced by both the electronic and nuclear factors, which are exponential in nature (in either separation distance or energy). As such, a wide range of ET reaction rates can occur from the second to picosecond regime. The main goal of this section is to describe the strategy for computing the electronic (T_{DA}) interaction between protein ET pairs that have docked in a given geometry. We also describe some qualitative features of the intermolecular docking energetics.

A. The Tunneling Pathway Model of Protein Mediated Electron Transfer

We now consider how one might approximate the ET rate constant for a given, fixed donor−acceptor geometry. To begin with, we will focus on the electronic contribution to the rate. The Franck−Condon analysis is discussed in detail elsewhere.[42] In many of the reactions considered here, the Franck−Condon factor is held nearly fixed, and differences between ET rates are likely to arise from differences in T_{DA}.

Assuming that a "tube" of orbitals between the donor and acceptor sites dominates the electronic coupling, the tunneling matrix element can be written in a pathway approach as[43−49]

$$T_{DA} = A \prod_i \epsilon_i^{bond} \prod_j \epsilon_j^{H-bond} \prod_k \epsilon_k^{space} \qquad (20)$$

More recently, new approaches by us[50−55] and by others[56−59] have improved upon this simple strategy. These more advanced methods have validated the basic assumptions of the pathway model, which are based simply upon the qualitative difference between through-bond and through-space wave function propagation, represented in the parameters of eq 20.[43−49] A description of this model and its extensive application in protein ET appear in refs 9, 43−49, and 61−65.

Physically, the decay through a "single" pathway should be understood to mean that coupling through a "tube" of bonds dominates the tunneling matrix element.[43−54] That is, many orbitals in the medium intervening between donor and acceptor contribute (in a rather complex manner) to the D−A coupling, but the overall value can be approximated using eq 20. Scattering of the propagating wave function amplitude through orbitals in the core of this tube, as well as by orbitals appended to this core pathway, are all incorporated by the choice of the decay parameters. This kind of interference, however, is called trivial interference. For example, the coupling provided by a protein backbone is a much stronger function of backbone length than it is of the types of residues encountered along the backbone. The amide hydrogens, lone-pairs, carbonyls, even the side-chain residues themselves provide alternative pathways that interfere in a way that can easily be included in a much simpler set of effective states with the connectivity of a string of pearls.[43−54] Even though renormalized (effective) parameters are used, the final coupling still can be described by a decaying product through this core pathway. All of the scattering effects within the tube can be included through effective parameters for the core orbitals; i.e., when one gives a decay per bond value (and the related picture), all of these effects are included. This

renormalization procedure to obtain effective parameters has been formally developed by us in several recent papers.[50−54] A *pathway tube* is the set of orbitals defined by a single core physical pathway (the set of interacting covalent bonds between D and A that defines the single strongest coupling pathway), adding to this set all nearest neighbor interacting orbitals, and finally adding the neighbors of these neighbors. This procedure captures all relevant orbitals that are off the core physical pathway, and this subset of the bridge is called a *pathway tube*.

The *single* pathway description will break down if multiple tubes are important in the mediation of the electronic coupling. In such a case, interference between tubes is a concern when predicting the donor−acceptor coupling. It is important, however, to distinguish *interferences between tubes* from trivial interferences or scattering within a single tube (described above). While the latter is important for the determination of the effective decay parameters, it does not modify the qualitative pathway concept. Another possible limit is that coupling is dominated by so many tubes that their interferences are important. In this regime, the independent tube description would break down and the protein could be thought of as an average medium in which details of the protein structure need not be important. Previous studies on chemically modified proteins have not yet shown such "average" behavior. New methods for predicting when a specific folded configuration will cause a protein to fall into one of these limiting regimes or another are under current investigation. Recent progress has been made to analyze the importance of specific contacts for the final coupling matrix element and to construct improved effective hamiltonians for electron transfer.[60,61] Qualitatively, it is easy to understand that when the coupling is dominated by a single tube, a few individual contacts can be of major importance. The importance of such specific contacts will decrease as more and more pathway tubes contribute to the coupling. The numerous protein and pathway analysis tools now available[5,50−54,56−59,62−66] provide a means of determining the pathway regime at play and the key contacts that mediate a specific protein ET reaction.

The single pathway picture has been remarkably successful in explaining electron transfer in numerous unimolecular and bimolecular protein ET experiments.[5,62−70] One of the most important examples is the family of chemically modified proteins studied by Gray and co-workers.[5,11,12,71] Rates of ET were measured between the native redox center inside the protein to a surface-histidine-bound ruthenium species. Time-resolved studies (luminescence quenching and flash−quench techniques) were used to measure the ET rates. In specific families of experiments, the donor and acceptor species were nearly the same, so the relative rates reflect T_{DA} rather directly. In a series of free-energy studies, Gray and Winkler[5,11,12] further modified the Ru site to estimate the activationless rates. Ratios of these activationless rates provide even better estimates of the relative tunneling matrix element values.

Experimental rates in the Ru−protein systems show that the simple model with an exponential decay with donor−acceptor separation is inadequate.

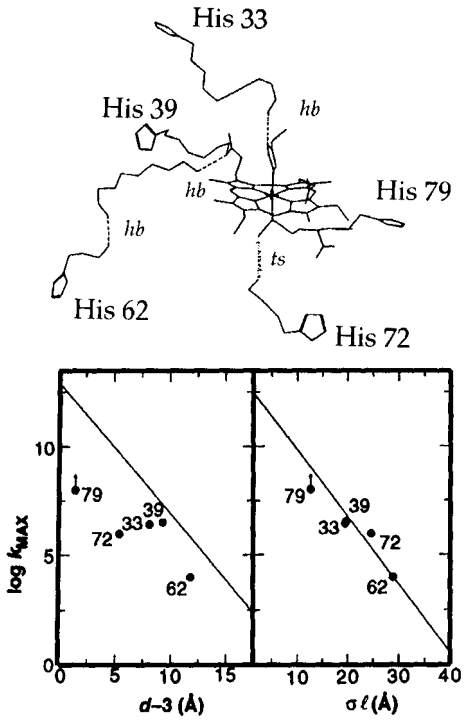

Figure V.1. Strongest coupling paths between the Fe and five different surface histidines examined in ruthenated C*c* experiments of Gray and co-workers.[5,11,12] Solid lines indicate covalent bonds, dashed lines show hydrogen bonds, and dotted lines show through-space contacts. The activationless electron transfer rates are plotted vs distance and length of the tunneling pathways. The tunneling path length, σ_L, is defined as the through-bond distance along an extended covalent chain that would produce a coupling decay equal to that arising from the specific strongest tunneling pathway in the system of interest. Note the improved fit when the activationless rates are plotted vs tunneling pathway length and the fact that the contact distance rate is $\sim 10^{12}-10^{13}$ s^{-1} in the pathway length correlation.

In one case, where a long through space jump exists in the main pathway, the tunneling matrix element is much smaller than one would otherwise expect for that donor−acceptor separation. This single pathway "tube" description fully explains the collection of rates in these modified cytochromes. More recent experiments and calculations in modified azurin provide examples where multiple tube effects appear.[5,62−66] Even though the tunneling matrix element is not a simple product of decay factors here, the pathway description for individual tubes still is the appropriate way to describe the protein mediation. Figure V.1 presents the strongest coupling paths from the Fe of C*c* to the five surface sites examined by Gray and co-workers.[72] In this figure, the experimental rates were measured as a function of two distances, the conventional physical separation between the donor and acceptor sites and the equivalent covalent distance. For a given coupling between D and A, the equivalent covalent distance provides the length of the chain if D an A were fully covalently coupled. If through space occurs in the dominant pathway, because the decay through space is much stronger, this jump will provide a much larger contribution to the covalent distance than its own length. This is exactly what happens to the Ru(His 72) C*c* case.

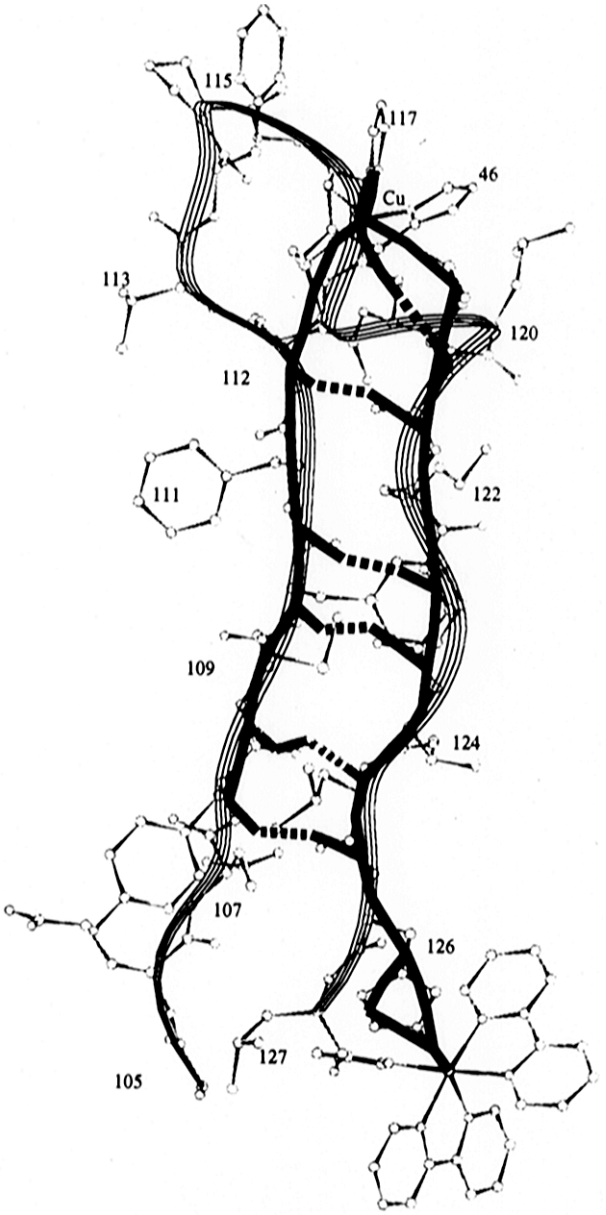

Figure V.2. Pathway tubes between the blue-Cu center and numerous ruthenation sites in modified azurin.[52,65] Rates to residues 107 and 109 are dominated by a single tube, while coupling between Cu and residues 122, 124, and 126 involve multiple tubes, leading to important interference effects not incorporated in a single path calculation.

The utility of the the pathway approach, as a guide to interpretation, is not lost even when it breaks down, and the quantitative coupling estimates of eq 20 are poor approximations in the multitube regime. Figure V.2 shows pathway tubes for ET between the Cu- and Ru-sites in Ru-modified azurin. Five different Ru-sites are shown in this figure. Because the electronic coupling between the Cu and the protein is dominated by Cys 112, ET rates to residues 107 and 109 are dominated by the single tube shown in Figure V.2. The pathway model predicts the ratio of the rates between them very effectively. The situation changes when residues 122, 124, and 126 are considered. Since the coupling pathways of importance go through residue 112, one can now see a collection of equivalent pathways for each of them by choosing different hydrogen bonds. Since the pathways are equivalent, tube interference is constructive, and the pathway approach underestimates the coupling. Residues further down the strand will have more equivalent pathways and, therefore, larger constructive interference effects. Using our Greenpath approach,[50−54] we have quantified these effects, but just using the pathway description we have been able to understand the mechanism involved and predict the results qualitatively.

Using pathway calculations to determine the dominant core paths, the following strategy is used to determine the tubes. The pathway "tube" is the set of bonds one finds by first identifying a core pathway (between some D and A) which never visits the same bond twice, then one adds to this set all nearest neighbors of the core bonds and then again adds the neighbors of these extra bonds. This captures all hanging orbitals off of the core pathway, and this subset of the bridge is called the pathway "tube". Green's function calculations are then performed using the "tube" orbitals and the full protein. In all calculations performed for C*c* and azurin, this reduced "tube" representation captures all the essential parts of the protein that contribute to the coupling.

B. Functional Docking

Determining the equilibrium distribution of docked protein geometries is a central challenge both in the experimental measurements of binding and in modern computational biophysical chemistry. We have defined a complementary view for thinking about the combined role of coupling pathways and binding in ET complexes. Instead of beginning with a fixed complex geometry, we analyze the two proteins individually and estimate the electronic coupling between the two redox centers and the protein surfaces in each reaction partner. By analyzing the surface coupling maps for each partner, we can learn how sensitive the electronic coupling is to the docking geometry. If the protein surface has extensive areas with similar coupling magnitudes, this provides an indication of weak specificity for docking. In this case, there is no need to compute, precisely, the docking geometry if the goal is to compute the interprotein electronic coupling. Alternatively, if the surface maps present specific areas of strong coupling, the question arises of whether or not these specific sites are physiologically responsible for ET control in the complex. Comparison of the binding sites obtained from docking simulations or from experiments with those obtained from this approach should lead to a mechanistic understanding of these reactions. Phrased differently, two factors will control ET in these systems. One is the probability of binding in a given geometry and the other is the rate in this geometry. Since the final rate depends on both of these terms, it is not guaranteed that the most stable conformation is the one that controls the ET rate. Therefore, the comparison proposed above will allow us to estimate the contribution of each of these terms.

It is important to observe that the electronic coupling for a given geometry, if dominated by a single pathway tube, can be written as a product

$$T_{DA}^{(biomolecular)} = A[\prod_i \epsilon_i^{protein-I} \prod_j \epsilon_j^{protein-II}]\epsilon^{inter} \quad (21)$$

Functional docking analysis uses information about the surface coupling in both proteins, but it says nothing about the coupling between the proteins. For any tight contact between proteins, the interprotein coupling is likely to be about the same. However, there is no guarantee that the tube through the thermodynamically most-favored binding contact will include the dominant tube. The most favorable conformation for ET need not be the most stable. Thus, calculations for the full complex are needed prior to reaching final conclusions; the strategy described above provides the basis for attaining a broad understanding of the interprotein interactions because it provides the theoretical tools for analyzing data in such systems and for guiding future experiments. It is important to understand that all of the computational tools developed to analyze electronic interactions in single proteins can be used in the bimolecular problem, even though additional complications, described above, arise as well.

We have studied ET between the proteins cytochrome c_2 (Cc_2) and the photosynthetic reaction center (RC) using this strategy.[73] The electronic coupling decay between electron donor and acceptor can be separated into three parts: (i) the coupling from the cytochrome heme to the surface of the cytochrome, (ii) the coupling from the RC surface to the bacteriochlorophyll dimer, and (iii) the coupling from the surface of the cytochrome to the surface of the reaction center. As discussed above, calculating the coupling between the surface amino acids and the redox center allows the simple estimate of interprotein electronic coupling and, for a given docked structure, provides a functional criterion for evaluating that structure. Central to this strategy is the definition of protein surface. The main assumption is that an electron must tunnel through a surface residue to leave the protein. To generate a smoother surface that prevents atoms in border invaginations of the protein from being considered surface residues, this surface may be defined by rolling a spherical probe of radius 3 Å (instead of the standard 1.4 Å) along the protein surface. To examine the effect of docking on electron transfer in the RC, we generated surface coupling maps of the electronic coupling between the redox sites and solvent exposed atoms in each protein before docking occurred. When we analyzed the strongest path between the special pair and the surface residues on the RC, we found a large region with similar coupling to the special pair (Figure V.3).

The reactive surface of the RC is large, whereas Cc_2 has a small region with much stronger coupling than the rest of the surface. Thus, electron transfer out of the Cc_2 is likely to be highly specific, whereas electron transfer into the RC is probably less specific. From this analysis of the coupling surfaces, we can learn quite a bit about protein surface patches that could play important roles in interprotein ET, but one still has to deal with the problem of the coupling between the two protein surfaces. The functional docking strategy suggests which surface regions of the proteins one should dock in order to optimize the ET rate without addressing the question of docking complex stability.

C. Classical Electrostatics and the Encounter Surface

In this section we describe the analysis of the surface electrostatics of C*c* and C*c*P. In sections VI.G and VII this analysis is combined with the Pathway calculations to develop a unified theoretical view of this bimolecular ET reaction. In order to discover the most significant docking site(s) using theoretical methods, it is necessary to consider both locations that optimize the electrostatic interactions between the enzyme and the substrate and associations that lead to efficient ET pathways. We present an analysis of the docking sites and their relation to ET using both the ET Pathways approach[43−49] and the *encounter* surface approach[74] for docking based upon the classical electrostatic calculations obtained from the Poisson-Boltzmann equation.[75−78]

Electrostatic potentials were computed by iterating the finite difference solution of the linearized Poisson−Boltzmann (PB) equation

$$\vec{\nabla}\cdot(\epsilon(\vec{r})\,\vec{\nabla}\,\varphi(\vec{r})) - \epsilon(\vec{r})\,\kappa^2(\vec{r})\,\varphi(\vec{r}) + 4\pi\rho(\vec{r}) = 0 \quad (22)$$

where $\epsilon(\vec{r})$ is the position dependent dielectric constant, $\varphi(\vec{r})$ is the electrostatic potential, κ is the Debye−Hückel screening constant, and ρ is the interior charge density. The numerical methods for computing the potential are described by Honig and co-workers[75−78] and are implemented in the program DelPhi.[79,80] The PB equation enables one to account for the discontinuity in the dielectric constant across the protein surface, the roughness of this surface, and screening arising from ions in the medium. In the present calculations, a dielectric constant (ϵ) of 80 was assigned to the water-accessible regions. The interior of the protein was assigned $\epsilon = 2$. The calculations were performed using a 20 mM concentration of a 1:1 electrolyte and an electrolyte exclusion zone of 2 Å around the protein. Amino acid atomic charge assignments are based upon the Amber force field, which accounts for the charges of ionizable amino acids.

The electrostatic potential map generated using DelPhi was then used to generate the *encounter* surface following the procedure given by Tiede and co-workers.[74] This *encounter* surface was computed with a 5 Å Connolly surface. Connolly surfaces generated in this manner have been of use to predict interprotein docking sites when limited rearrangement of protein side chains occur upon interaction. The Connolly surface can also be used to search for regions of complementary electrostatic potentials in the bimolecular complexes that do not depend upon specific charge pairing or mutual rearrangement of side chains. Such surface regions are relatively insensitive to the precise positions of amino acids.

*VI. ET between the Physiological Partners, C*c* and C*c*P*

As an illustration of the ideas presented above, we consider ET between the physiological partners C*c*P and C*c*. C*c*P is found in the periplasmic space of yeast mitochondria and catalyzes the two-electron reduction of H_2O_2 by two molecules of Fe^{2+}C*c* as the specific electron source.[17,81−83]

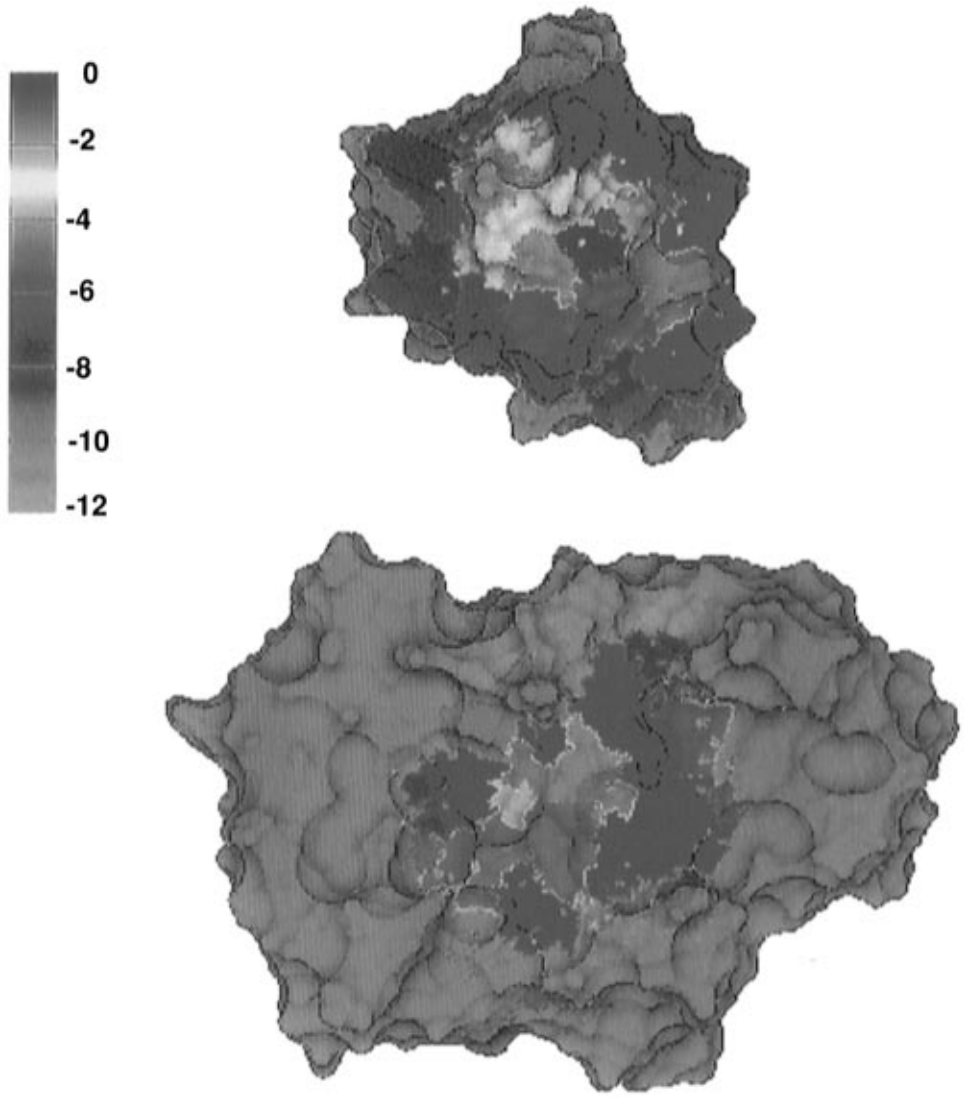

Figure V.3. Electronic coupling surfaces, computed from the pathway model, from the chlorophyll special pair to the surface of the RC and and from the heme of cytochrome c_2 to the protein surface. Electrons transferred from cytochrome c_2 to the special pair of RC fill the hole left following photoinduced charge separation in the RC. Note the broad strong coupling surface on the RC and the narrower strong coupling surface on cytochrome c_2. (Scale is logarithmic.)

$$H_2O_2 + 2Fe^{2+}Cc + 2H^+ \rightarrow 2Fe^{3+}Cc + 2H_2O \quad (23)$$

In the first step of the C*c*P catalytic cycle, the ferriheme resting state of C*c*P undergoes a two-electron oxidation by H_2O_2 (eq 24). The first stable

$$Fe^{3+}CcP + H_2O_2 \rightarrow ES \quad (24)$$

$$ES + Fe^{2+}Cc \rightarrow CcP\text{-}II + Fe^{3+}Cc \quad (25)$$

$$CcP\text{-}II + Fe^{2+}Cc \rightarrow Fe^{3+}CcP + Fe^{3+}Cc \quad (26)$$

species produced in this reaction, historically denoted compound ES, is oxidized by 2 equiv above the resting state. In this high-valence intermediate, one oxidizing equivalent is stored as a ferryl iron-oxo $[Fe^{IV}{=}O]^{2+}$ species and the other as a radical on Trp 191.[84−86] To complete the catalytic cycle, one molecule of Fe^{2+}C*c* reduces ES by 1 equiv to form C*c*P-II (eq 25) which, is then reduced by a second molecule of Fe^{2+}C*c* to the resting state (eq 26).

The first reduction step can occur *either* at the heme or the Trp radical, and thus C*c*P-II exists in two electronic configurations that are 1-equiv oxidized relative to the ferriheme resting state, one with an oxidized heme (C*c*P-II_h) and one with an oxidized Trp (C*c*P-II_r).[87−90] These two forms exhibit a pH-dependent equilibrium[89,91] and the oxidizing equivalent can transfer between the two redox sites through an intramolecular ET process that is not fully understood and can be surprisingly slow.[87,88,92] Because this catalytic cycle involves two C*c* molecules and two spatially and electronically distinct redox centers of C*c*P, the key question is whether the reductions occur by sequential reactions at a single binding domain on the C*c*P surface or whether there might be two ET-active domains, opening the possibility that there are even different "pathways" for heme and Trp reduction.

A. One Structure for the [C*c*P, C*c*] Complex?

C*c*P is an acidic protein having a net negative charge at pH 7.0. In 1980[93] the crystal structure of C*c*P revealed that the surface of C*c*P surrounding the edge of the heme that bears the heme propionates contains a large number of negatively charged amino acids. Cytochromes *c* generally are basic proteins with net positive charges at pH 7, and it was shown

in 1971 that these two proteins can form a complex through forces that are predominantly electrostatic.[94] Margoliash and co-workers showed that modification of specific Lys residues on the surface of C*c* inhibited its reaction with C*c*P, which led to the hypothesis that docking to C*c*P involves the ring of positively charged Lys residues surrounding the exposed edge of the heme crevice on the "front" surface of C*c*.[95,96] To locate the binding site for C*c* on the surface of C*c*P, Bechtold and Bosshard[97] compared the reactivity of surface carboxyl groups in free peroxidase to their reactivity in the presence of C*c*.

The possible significance of the high degree of complementarity between the region of positively charged Lys of C*c* and the negatively charged residues of C*c*P led to attempts to use computer studies to visualize the [C*c*P, C*c*] complex. The first computer-generated structure of the 1:1 complex[98] was obtained by manipulating the X-ray structures of the two component proteins to achieve optimal hydrogen-bonding distances and geometries between pairs of negatively charged Asp residues of C*c*P and the positively charged Lys residues of C*c*. The intervening medium is comprised of portions of the two protein polypeptides and includes Phe 82 of C*c* and His 181 of C*c*P. On the basis of this structure it was proposed that the pathway for heme−heme ET involved $\pi-\pi$ superexchange interaction between His 181 of C*c*P and Phe 82 of C*c*.

The structure of a 1:1 complex studied crystallographically by Pelletier and Kraut[99] shows a C*c* bound at roughly the same region as proposed by modeling, but with rather different contacts and relative orientations of the hemes. According to the high-salt crystal structure of the [Fe^{3+}C*c*P, Fe^{3+}C*c*-(yeast iso-1)] complex, pyrrole ring C of C*c* is in close contact with residues Ala 193 and Ala 194 of C*c*P. The shortest ET pathway connecting this corner of the heme to the heme of C*c*P travels along the backbone of C*c*P and passes through residues Ala 194, Ala 193, Gly 192, and Trp 191.[72] The latter, of course, is the radical site and is in van der Waals contact with the peroxidase heme. According to the Pelletier−Kraut structure, the dominant interactions between Fe^{3+}C*c*P(MI) and Fe^{3+}C*c*(yeast iso-1) include van der Waals forces and hydrogen bonds, rather than predominantly electrostatic interactions, as proposed earlier by Poulos and Kraut[98] and as inferred from solution studies. Given that the crystals were partially dried prior to diffraction measurements, the precise relationship between the diffraction results and protein−protein interactions that are significant in solution is uncertain. Nonetheless, publication of the hypothetical structure of the [Fe^{3+}C*c*P, Fe^{3+}C*c*(tuna)] complex by Poulos and Kraut in 1980 and the subsequent solution of the X-ray crystal structure of [Fe^{3+}C*c*P(MI), Fe^{3+}C*c*] complexes by Pelletier and Kraut in 1992 provided a groundbreaking glimpse of the static structure of such complexes.

Results from H/D exchange experiments have been used to compare the crystallographic structure with the structure of the complex in solution.[100,101] Hydrogen−deuterium exchange labeling of the backbone amide protons of Fe^{3+}C*c* in both the C*c*P-bound state and the free state has been used to map the binding site of C*c*P on C*c*. The interface region identified by comparing the H/D exchange rate constants of the free and bound states is similar to the binding interface obtained from the solid-state crystal structure. However, a second protected region located away from the crystallographically derived interface and encompassing the "back" side of C*c*(yeast) also was detected, evidence for the existence of a second binding domain. The protection factors for H/D exchange are significantly smaller for the [C*c*P, C*c*(horse)] complex than for [C*c*P, C*c*(yeast)], evidence that the details of complex formation are different for the two cytochromes.

Chemical cross-linking reagents have been used to covalently link C*c*P and C*c*.[102−105] Cross-linking reactions are generally nonspecific and generate multiple products. Separation and characterization of these products are tedious and time-consuming. Studies with these covalent complexes show that if the spacer is too long, the complex can be quite flexible so that the distance between the redox centers can be difficult to determine and may, in fact, exceed the separation that is achieved by the non-covalent, electrostatic complexes. For these reasons, a focal point of this research has involved the design of new cross-linking reagents with the intent of minimizing the length of the linker molecule so as to obtain maximum rigidity within the covalent complex.

Today the conventional chemical modification strategy is being applied in more elegant ways using molecular biology to genetically modify surface residues that are not easily modified using conventional chemical modification reagents. Aided by the electrostatic model and the crystallographic structure, new molecules are being designed to probe the specific interactions that define the protein−protein interface. Preparation of 1:1 complexes that have been covalently coupled at specific sites created by site-directed mutagenesis provides a new strategy for mapping the structure of the interface and studying the dynamics of the protein−protein complex as they pertain to ET. With advances in molecular engineering, one can manipulate the attachment site with relative ease by introducing a specific target site for the cross-linking reagent. Wang and Margoliash[106] have prepared mutants of C*c* that will bind cross-linking reagent at a specific site on C*c*, while not restricting the cross-link to a specific site on C*c*P. Poulos and co-workers[107,108] have taken this strategy one step further and prepared covalent complexes in which there is a unique site on both C*c* and C*c*P for cross-linking. In this approach, the "zero-length" cross-link is an intermolecular disulfide bond formed by mixing mutants of C*c*P having a single Cys residue with a mutant of C*c* that also has a single Cys residue. Such restricted mobility may, however, mask the conformational dynamics that are significant for optimal ET. Thus, the ultimate test of the significance of any chemical or biochemical modification requires kinetic measurements, and the interpretation of such measurements must necessarily include a study of binding and dynamic processes.

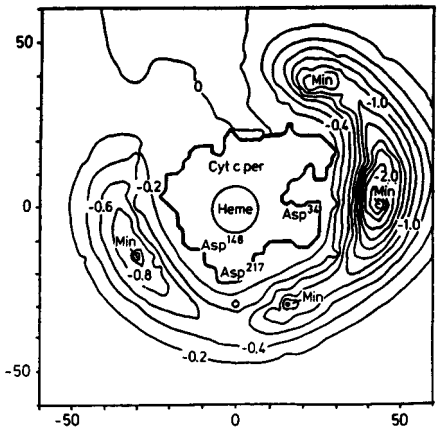

Figure VI.1. Electrostatic potential energy contour plot for the interaction of Fe^{3+}C*c*P and Fe^{2+}C*c*(tuna) as a function of the center of mass position of the cytochrome. The cross section is through the heme plane of C*c*P. The primary binding domain centered near Asp 34 on the "right" includes three overlapping sites. A second domain, located to the "left" of the heme, that has not been observed crystallographically is centered near Asp 148. The figure has been adapted from refs 109 and 110.

B. Dynamic View—Experimental Evidence for Multiple Conformations

Crystallographic studies provide a static snapshot of a single form of the complex. However, the Brownian dynamics simulations of Northrup and coworkers[109−112] graphically suggested that more than one conformation of the [C*c*P, C*c*] complex may be accessible. As seen in Figure VI.1, several discrete and energetically accessible energy minima are suggested for the binding of C*c* on the surface of C*c*P. The most stable minimum is that found by Poulos and Kraut and overlaps with the structure found by Pelletier and Kraut. However, it appears not to be the one with the smallest metal−metal separation, consistent with the possibility that conformational processes influence and/or control ET.

In fact, considerable experimental evidence suggested that the thermodynamically most stable electrostatic complex is *not* optimally configured for ET and that rearrangement of the proteins within the complex is necessary for efficient ET. For example, at an equimolar C*c*/C*c*P ratio, where is it universally agreed that only 1:1 binding is significant, ET is inhibited at low ionic strength[102,113] but becomes more efficient when the ionic interactions are masked either by increasing the ionic strength or through interface mutations on the C*c*. Furthermore, the rate constant for ET in a 1:1 cross-linked complex is less than the maximum rate constant for the noncovalent complex.[102] Both results can be explained by conformational gating[15,41] of ET through movement of C*c* among several sites on the surface of C*c*P.

Low-temperature measurements of triplet-state quenching rate constants[114,115] have directly revealed the importance of conformational interconversion for reactions within the complex between C*c*P and C*c*. As shown in Figure VI.2, the triplet decay traces for the quenching of ^{3}ZnP within ZnC*c*P by Fe^{3+}C*c* are rigorously exponential down to ∼250 K, but upon further lowering of the temperature, the triplet decay traces become nonexponential and the quenching abruptly vanishes. This phenomenon was interpreted as the manifestation of a novel intracomplex conformational transition. It has been modeled as a "phase transition" between a thermodynamically stable, but inactive, low-temperature conformation and a high-temperature, active form. This process may well prove to be a paradigm for interfacial regulation of interprotein interactions. A reinvestigation of this process using a combination of metal substitution and site-directed mutagenesis should unravel the structural features involved in this transition. It has also been found that the kinetic progress curves describing the thermal back ET from Fe^{2+}C*c* to the π-cation radical of ZnC*c*P behaves in a manner consistent with gated ET.[116]

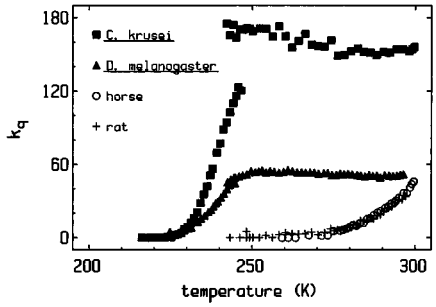

Figure VI.2. Temperature dependence of the triplet quenching rate constant for complexes of ZnC*c*P with C*c* from several species.

C. New Titration Strategies Show That C*c*P Has Two Binding Domains

The most direct demonstration that ET between C*c* and C*c*P could occur at distinct domains on the C*c*P surface would be to show that C*c*P could actually bind two C*c* to form a ternary complex. During the more than 2 decades since it was first shown that C*c*P and C*c* form a complex at low ionic strength,[94] the stoichiometry of binding was a matter of some dispute. The formation of a 2:1 complex at low ionic strength was first indicated by size-exclusion chromatography,[117] the first molecule binding with a high affinity and the second with a much lower affinity. Furthermore, the steady state kinetics with eukaryotic C*c* are biphasic at low ionic strength, leading to a model of C*c*P with two catalytically active sites.[117] Nonetheless, it was the general consensus that only a 1:1 complex was formed.[118−124]

This consensus held until 1993, when studies of the photoinduced ET between ZnC*c*P and Fe^{3+}C*c* revitalized the idea that a 2:1 complex, and thus two binding domains, is biologically significant.[18] For the studies with ZnC*c*P (C-type heme substitution), the thermal back reaction (eq 2) is a structurally and functionally faithful model for heme reduction of both compound ES and C*c*P-II$_h$ in that it involves ET between the ferroheme of Fe^{2+}C*c* and the oxidized ZnP heme of ZnC*c*P. Such studies, using cytochromes from a variety of species as well as cytochrome surface mutants, helped to initiate the modern wave of studies of long-range ET.[27,28,116,125] In experiments with ZnC*c* (I-type heme substitution), which is a structural and electrostatic analog of Fe^{2+}C*c*, photoinitiated ET from ZnC*c* to the ferri−heme of resting state C*c*P is a comparably excellent model for the reduction of the heme site in ES and C*c*P-II$_h$.[19,126] A key virtue of using Zn-substituted

proteins to study the reactions of C*c*P is that they simplify the complicated problem presented by the presence of the two redox-active centers in C*c*P and of the two interconverting forms of C*c*P-II. By eliminating the oxidized Trp as a possible participant in most or even all of the reactions, one isolates and can cleanly address questions of binding and interfacial dynamics. Once these are understood, one can begin to characterize the heme−heme ET event itself, without complication from the involvement of the Trp radical and interconversion between the two forms of C*c*P-II. The processes that involve the Trp then can be addressed by the complementary technique of surface-bound metal complex,[33,34] and the results embedded in the overall picture of binding, docking, and heme−heme reactivity can be obtained from the heme substitution experiments. However, as we now discuss, progress in obtaining this picture required the use of the new experimental strategies explained in section IV above.

Combining Quenching and ET-Product Detection

The first heme substitution experiments to study the complex between C*c*P and C*c* employed the C_N titration protocol in which Fe^{3+}C*c* as quencher (S) was titrated into a solution containing a fixed concentration of ZnC*c*P as the ET photodonor ($E^\dagger$).[18] The early studies[27,28] in which quencher was only added to a moderate excess disclosed (Figure VI.3) a break in the curves at $R = [Fe^{3+}Cc]/[ZnCcP] \sim 1$. When higher values of R were used, it was found that this break is followed by a further gradual increase in Δk for $R > 1$.[18] The break in behavior at $R \sim 1$ clearly shows that C*c*P tightly binds one molecule of C*c*. The subsequent gradual increase could represent binding of a second C*c* with a low affinity. However it could equally well reflect nonspecific, collisional Stern−Volmer quenching of the excited state 1:1 complex by a second molecule of C*c* without formation of a 2:1 complex. It is not possible to distinguish between these two alternatives through use of the C_N quenching protocol alone. However, this was achieved by correlating measurements of ET quenching with direct observation of the [ZnP^+C*c*P, Fe^{2+}C*c*] charge-transfer intermediate (I) produced by the quenching (eq 1).[18] The observation that the appearance of the ET intermediate lags behind the triplet quenching, with appreciable formation occurring only for [C*c*]/[C*c*P] > 1 (Figure VI.3), was interpreted to result from the formation of a 2:1 complex, where one Fe^{3+}C*c* binds to a high-affinity domain that is ET-inactive (but exhibits strong energy-transfer quenching), while the second cytochrome binds to a low-affinity domain that allows efficient ET quenching. The observation that raising the ionic strength[18] eliminates most of the ET quenching but not that from energy transfer confirmed that ET occurs preferentially at the low-affinity domain, which is less sensitive to ionic strength.

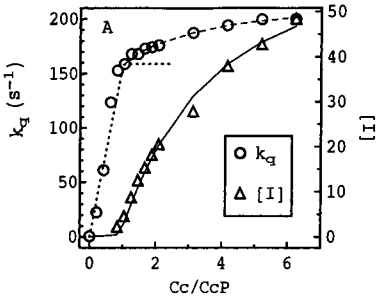

Figure VI.3. Triplet quenching (○) and yield of the ET intermediate (△) for a C_N titration in which Fe^{3+}C*c*(*Candida kruseii*) is added into a solution of ZnC*c*P. The dotted line is a simulated 1:1 binding isotherm ($K = 0.001$ μM, $k = 159$ s^{-1}). The dashed line is a fit of the quenching profile at $R \geq 1$ to a 2:1 binding isotherm assuming $K_1 = 0.001$ μM and $k_1 = 159$ s^{-1} ($K_2 = 10$ μM and $k_2 = 60$ s^{-1}). The solid line through the [I] data is a fit to a 2:1 binding isotherm assuming the quenching for the first binding step arises from $^3ZnP \rightarrow Fe^{3+}P$ Förster energy transfer so that the high-affinity step is ET-inactive. $K_1 = 0.001$ μM, $k_1 = 0$, $K_2 = 10$ μM. Conditions: 5 μM ZnC*c*P, 1.0 mM KP_i buffer (pH 7.0), 20 °C.

Experiments of this type were used to compare the binding affinities of fungal C*c* and mammalian C*c* for ZnC*c*P.[18] The fungal C*c* show higher quenching at the strong binding domain than the nonfungal C*c*.[18,115] This dependence of the reactivity and affinity on the identity of the C*c* likely reflects subtle differences in the structures of the two classes of complexes, and indeed, slight differences were detected in the X-ray crystal structures of the 1:1 complexes of Fe^{3+}C*c*(yeast iso-1) and Fe^{3+}C*c*(horse) with Fe^{3+}C*c*P.[99]

The time-resolved kinetic profiles obtained during such C_N titration experiments with MgC*c*P have been used to study the dynamics of complex formation at the strong binding domain.[127] The rate constant for dissociation of Fe^{3+}C*c*(yeast iso-1) from the strong binding is much less than the rate constant for dissociation from the weak binding domain. Similar experiments with Fe^{3+}C*c*(horse) showed that dissociation from both the weak and the strong binding domains is fast compared to the rate of intracomplex ET.

New Titration Protocols at Low Ionic Strength

The inverse heme substitution strategy[19] and reverse-titration protocol[126] were developed as part of an effort to test the conclusion that C*c*P binds C*c* at two nonexclusive domains. Figure VI.4 presents an

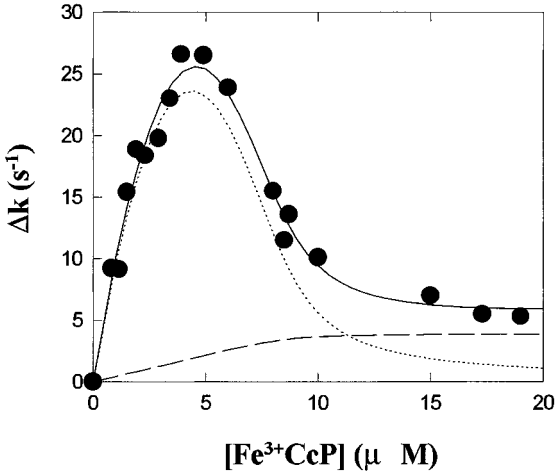

Figure VI.4. I_N titration of ZnC*c*(horse) by Fe^{3+}C*c*P. The solid line is the fit to the 2:1 binding isotherm. Stoichiometric binding parameters are given in Table VI.1. The dotted line shows the contribution to the quenching from 1:1 complexes and the dashed line is the contribution from the 2:1 complex. Conditions: [ZnC*c*] = 8.5 μM, 2.5 mM KP_i buffer (pH 7.0); 20 °C.

Table VI.1. Domain Constants for 2:1 Binding of ZnC*c* by Fe^{3+}C*c*P Estimated from the Stoichiometric Constants Obtained from an I_N Titration at 4.5 mM Ionic Strength, pH 7.0, and 20 °C

K_{10} (M^{-1})	K_{20} (M^{-1})[a]	K_{12} (M^{-1})	K_{21} (M^{-1})	^1k (s^{-1})	^2k (s^{-1})
7.7×10^6	$<1.9 \times 10^4$	7.5×10^3	3.0×10^6	<2.4	1620

[a] $K_{20} > K_{12}$.

I_N titration in which a fixed amount of ZnC*c*(horse) as photoprobe ($S^\dagger$) is titrated with increasing aliquots of the quencher, Fe^{3+}C*c*P (E), at low ionic strength ($\mu = 4.5$ mM). In this titration, the quenching rate constant increases with addition of quencher, reaches a maximum value near [ZnC*c*]/[Fe^{3+}C*c*P] = $^1/_2$, and then decreases with subsequent additions of Fe^{3+}C*c*P. This shape could not arise with a simple 1:1 stoichiometry. Rather, it reflects quenching in which the 2:1 ternary complex ($ES_2^\dagger$) dominates ($k_2 \gg k_1$) and thus quenching follows the f_2 surface as plotted in Figure IV.8. Such a result demonstrates *unambiguously* that at low ionic strengths C*c*P can simultaneously bind C*c* at two *distinct* domains with highly different affinities and reactivities. Analysis of the characteristic shape of this titration curve according to eq 13 yielded precise values of the stoichiometric rate constants and the stoichiometric affinity constants. Estimates of the domain parameters that are compatible with the stoichiometric parameters are given in Table VI.1.

These measurements are complemented by a C_R titration in which the probe (ZnC*c*P, $E^\dagger$) is added to a solution of Fe^{3+}C*c*(horse) (S) in 5 mM KP_i buffer (pH 7) (Figure VI.5).[128] In this experiment, the observed quenching rate constant decreases upon addition of ZnC*c*P, regardless of stoichiometry. However, as discussed above, the sharp drop in Δk that occurs as $R = [E^\dagger]/[S]$ approaches 1:1 indicates that

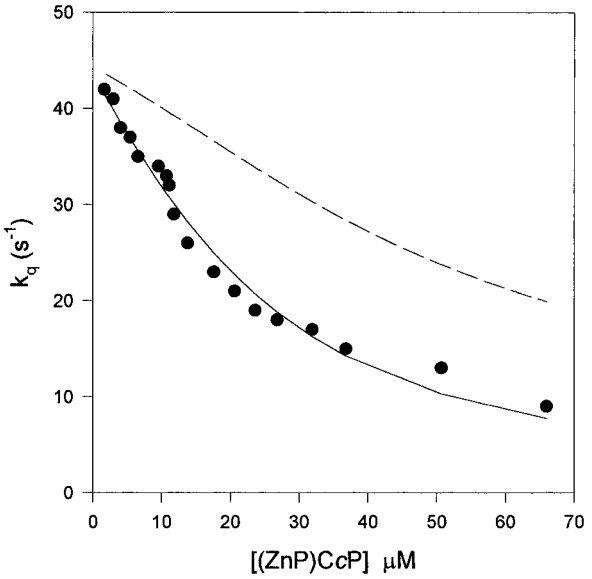

Figure VI.5. C_R titration of Fe^{3+}C*c*(horse) by ZnC*c*P. The solid line is a three-parameter fit to the 2:1 binding isotherm. Stoichiometric parameters: $k_1 = 16$ s^{-1}, $K_1 = 1.6 \times 10^6$ M^{-1} (Calculated from the measured value of $\Delta k_0 = 43$ s^{-1} and the three fitting parameters, k_2, K_2, and k_1), $k_2 = 408$ s^{-1}, $K_2 = 5.4 \times 10^3$ M^{-1}. The dashed line is a simulation for 1:1 binding using the parameters obtained by fitting a C_N titration with a 1:1 binding isotherm ($K = 7.4 \times 10^4$ M^{-1} and $k = 67$ s^{-1}). Conditions: [Fe^{3+}C*c*(horse)] = 25 μM, 5.0 mM KP_i buffer (pH 7.0), 20 °C.

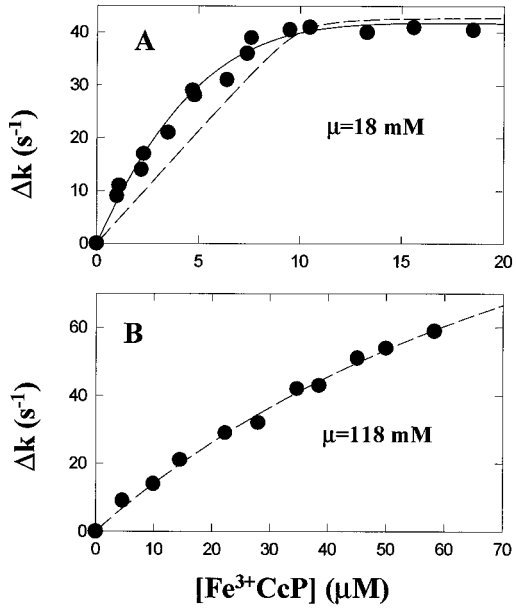

Figure VI.6. I_N titrations of ZnC*c* by Fe^{3+}C*c*P as a function of ionic strength. Conditions: $[ZnCc]_0 = 10$ μM, KP_i buffer (pH 7.0), 20 °C. (A) $\mu = 18$ mM. The solid line is the best fit to the 2:1 binding equation. Stoichiometric binding parameters are given in Table VI.1. The dashed line is a simulated curve for 1:1 binding: $K = 5 \times 10^7$ M^{-1}, $k = 43$ s^{-1}. (B) $\mu = 118$ mM. The dashed line is the best fit to the 1:1 binding equation: $K = 1 \times 10^4$ M^{-1}, $k = 170$ s^{-1}.

two molecules of C*c* can simultaneously bind to C*c*P. The 2:1 complex contributes to Δk for $R < 1$, and the nonzero value of Δk_0 allows a more precise estimate of the stoichiometric constants describing the second binding step.

High Ionic Strength

With 2:1 stoichiometry having been established for low ionic strengths, the next question is whether reactions at two domains occur at higher, physiologically relevant ionic strengths, $\mu \geq 100$ mM. When the I_N titration is done at slightly higher ionic strength (18 mM) (Figure VI.6), the titration curve again departs from the hyperbola expected for a 1:1 binding stoichiometry, but the difference between the titration curves for the 1:1 and 2:1 binding models is sharply reduced. At 118 mM ionic strength, however, the I_N titration gives no evidence for a 2:1 complex (Figure VI.6). Instead, the dependence of Δk on Fe^{3+}C*c*P quencher concentration can be described extremely well by a 1:1 binding equation.[126]

Establishing the binding stoichiometry and influence of the second domain at higher ionic strength required I_R titrations, where ZnC*c* ($S^\dagger$) as the titrant is added to Fe^{3+}C*c*P (E) as quencher.[126] Figure VI.7 shows I_R titrations at three ionic strengths. In the experiment at $\mu = 4.5$ mM, there is a low value for the intercept, Δk_0. As shown in the lower panel of Figure IV.3, for 1:1 binding the quenching would *necessarily* decrease further during this reverse titration. Instead, there is a lag in Δk for $R = [ZnCc]/[FeCcP] < 1$, and then Δk *increases* with increasing additions of ZnC*c*. This lag occurs because when Fe^{3+}C*c*P is in excess (R < 1), essentially all the ZnC*c* molecules form a 1:1 complex which has low reactivity. Quenching increases upon further additions of ZnC*c* (R > 1) because the additional ZnC*c* binds to

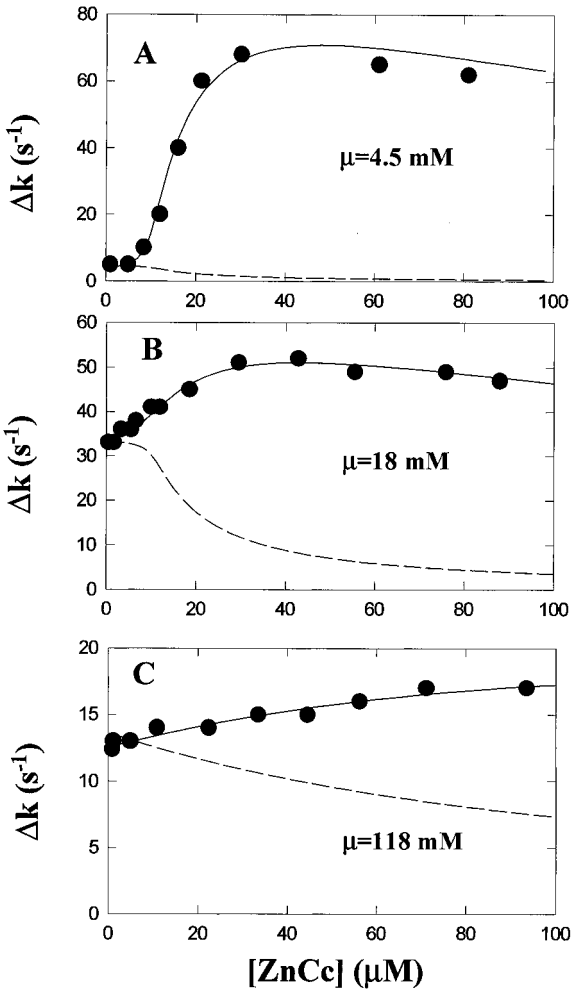

Figure VI.7. I_R titrations of Fe^{3+}C*c*P by ZnC*c*(horse) as a function of ionic strength. The solid lines represent the best fit to the 2:1 binding isotherm. The stoichiometric constants are summarized in Table VI.2. The dashed lines are theoretical curves generated for 1:1 binding. Conditions: (A) $\mu = 4.5$ mM, $[Fe^{3+}CcP]_0 = 10$ μM. Kinetic constants for the 1:1 simulation: $K = 5 \times 10^7$ M^{-1}, $k = 4$ s^{-1}. (B) $\mu = 18$ mM, $[Fe^{3+}CcP]_0 = 10.4$ μM. Kinetic constants for the 1:1 simulation: $K = 5 \times 10^6$ M^{-1}, $k = 38$ s^{-1}. (C) $\mu = 118$ mM, $[Fe^{3+}CcP]_0 = 10$ μM. Kinetic constants for the 1:1 simulation: $K = 1 \times 10^4$ M^{-1}, $k = 170$ s^{-1}.

Fe^{3+}C*c*P to form a highly reactive 2:1 complex. The quenching eventually falls because the fraction of the total ZnC*c* that is bound in the 2:1 complex decreases as the titration proceeds. Thus, the data confirms the presence of two binding domains and the functional importance of the ternary (2:1) complex at this low ionic strength. Figure VI.7 also presents I_R titrations at 18 and 118 mM ionic strengths. In both cases, parameters that best describe the I_R titrations at the corresponding ionic strengths require that Δk decrease over the course of the reverse titrations. Instead, Δk *increases* during the initial phases of both titrations and actually shows a maximum during the titration at 18 mM ionic strength. The explanation for these results is the same as for the titration at 4.5 mM ionic strength; again, the experimental data cannot be described by 1:1 binding but can be well fit with a 2:1 model. Thus, the I_R experiments confirm the functional importance of two binding domains and the presence of the ternary (2:1) complex at physiological ionic strength.

Table VI.2. Stoichiometric Constants[a] for 2:1 Binding of ZnC*c*(horse) by Fe^{3+}C*c*P as a Function of Ionic Strength[b]

μ (mM)	K_1 (M^{-1})	K_2 (M^{-1})	k_1 (s^{-1})	k_2 (s^{-1})
4.5	8.8×10^6	7.6×10^3	4.2	1560
18	8.5×10^5	4.3×10^3	38	1540
118	6.6×10^3	1.4×10^3	200	2000

[a] The average of I_N and I_R values. [b] pH 7.0, 20 °C.

Analysis of the I_N and I_R curves shows that the two stoichiometric binding constants change differentially with ionic strength (Table VI.2). This requires an accompanying change in the distribution of the singly bound C*c* between the two binding domains on C*c*P, namely a change in the relative amounts of the [^{1}ES] and [^{2}ES] forms of the 1:1 complex (Scheme III.2). The stoichiometric ET rate constant of the 1:1 complex (k_1) increases with increasing ionic strength, whereas the stoichiometric ET rate constant of the 2:1 complex (k_2) is almost insensitive to changes in ionic strength. The changes in k_1 are best interpreted as reflecting changes in the $^ig_1$ weighting factors that result from changes in the binding constants (eq 14); the constancy of k_2 suggests that the domain rate constants are insensitive to ionic strength (eq 15).

As a result of the changes in the K_i, the 1:1 complex contributes increasingly more to the overall reactivity as the ionic strength approaches physiological values. Because the differences in affinity and reactivity diminish with increasing ionic strength, it becomes more difficult to discriminate between a 1:1 binding model and a 2:1 binding model. Only with the reverse titration, where ZnC*c* is the titrant, was it possible to clearly demonstrate the presence of the 2:1 complex at physiological ionic strengths and to extract reliable stoichiometric parameters.

Variations in the binding of C*c* to C*c*P as a function of ionic strength indicate that there are strong electrostatic interactions within the binding interface. Table VI.2 shows that electrostatic interactions are more significant for the first binding step than for the second binding step. This difference in the electrostatic properties of the two binding steps likely arises because binding of the first C*c* involves interaction of two highly charged proteins having opposite polarity, whereas binding of the second C*c* to the 1:1 complex involves interaction between the positively charged C*c* and a weakly charged complex.

D. Interactions between the Two C*c*P Binding Domains?

The conclusion that C*c*P binds C*c* at two distinct domains, with greater reactivity for the 2:1 complex than for the 1:1, could mean that the high-affinity domain itself has intrinsically low reactivity for heme−heme ET, while the weakly binding domain has high reactivity, but it also is possible that the domain reactivities themselves are altered when the second C*c* binds. The simplest, limiting 2:1 kinetic model would involve binding and reaction at two independent domains (each possibly with multiple overlapping sites) (Scheme VI.1). However, C*c*P is too small to bind two C*c* without some interaction between them, and one must therefore consider "cooperativity" between the two bound C*c*. As we discussed in section III.B, one consequence of inter-

Scheme IV.1

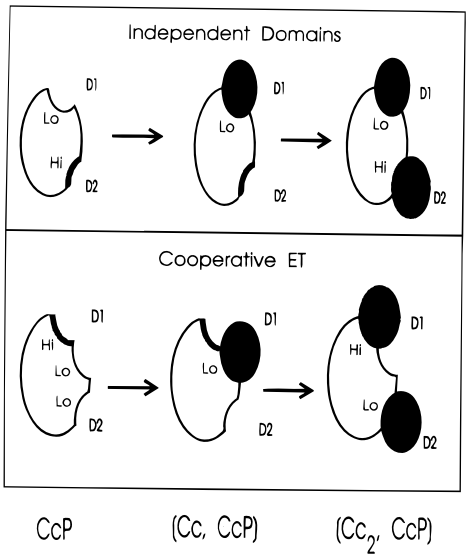

actions between domains is that the affinity of one domain changes when other domains are occupied. Measured stoichiometric constants provide no clue as to the extent of interdomain interactions. Wang and Margoliash[106] addressed this problem by preparing covalently linked, 1:1 complexes of C*c* and C*c*P. By studying the binding of a second C*c* to such a complex they could probe the interaction between the low- and high-affinity domains.

There are, in addition, other possible consequences of interactions. The first C*c* might bind tightly at one domain, but in a nonreactive conformation. This "tight" site could then become reactive upon binding a second C*c* at a nonreactive, "remote" site, in a model that recalls the proposal of substrate-assisted product dissociation[14] discussed in section VI.E. Such issues of binding specificity and of reactivity in protein−protein reactions are analogous to those in enzyme−substrate reactions, but studies of ET complexes have lacked parallels to the imaginative uses of substrate analogues and inhibitors in enzymology. We recently demonstrated[129] that this kind of fundamental mechanistic question about the reaction between protein ET partners can be resolved by the use of a metalloprotein that has been converted into a redox-inert, mechanism-based inhibitor through appropriate metal substitution. This strategy was illustrated by using Cu^{2+}-substituted C*c*[32] as a structurally faithful but redox-inert analog of Fe^{2+}C*c* to probe ET within the ternary complex. The utility of this probe is enhanced by using C*c* from multiple sources. Fungal C*c*, such as that from *Pichia membranefaciens* (*Pm*), have a greater affinity for C*c*P than those from vertebrates, and either type can be prepared with a selected metal ion: Fe, Zn, or Cu. Thus, it is possible to perform an experiment in which C*c*P preferentially binds a fungal metallo-C*c* having a selected metal and reactivity (Fe^{3+}C*c*, ET quencher; ZnC*c*, ET photodonor; and CuC*c*, inhibitor) in the presence of a vertebral C*c* with a different metal and a different reactivity.

Two types of titration experiments were performed where redox-inert CuC*c*(*Pm*) blocks the tight-binding domain on C*c*P from access by a redox-active C*c*-(horse); in one case the redox-active species was

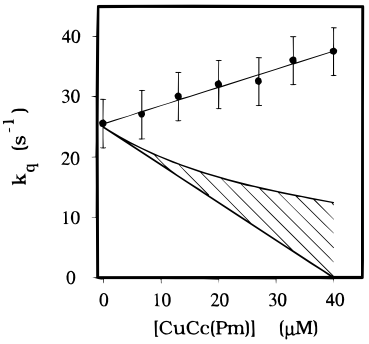

Figure VI.8. Titration of a 1:1 mixture of ZnC*c*P and Fe^{3+}C*c*(horse) by the inhibitor Cu^{2+}C*c*(*Pm*). The straight solid line is included to guide the eye. The shaded area represents the range of results that could be observed for 1:1 binding, with the upper boundary arising with equal affinities for Fe^{3+}C*c*(horse) and Cu^{2+}C*c*(*Pm*) and the lower boundary arising when Cu^{2+}C*c*(*Pm*) has a far higher affinity. Conditions: [ZnC*c*P] = [Fe^{3+}C*c*(horse)] = 40 μM, μ = 4.5 mM, pH 7.0, 20 °C.

ZnC*c*(horse) (I protocol), in the other it was Fe^{3+}C*c*(horse) (C protocol). Figure VI.8 shows the titration of an equimolar solution of ZnC*c*P and horse-heart Fe^{3+}Cc(horse) (pH 7.0, μ = 4.5 mM; 20 °C) by a solution of the CuC*c*(*Pm*) inhibitor. Prior to addition of inhibitor, photoinduced ET from ^{3}ZnC*c*P to Fe^{3+}C*c*(horse) is manifested in quenching with a rate constant of $\Delta k = 26\ s^{-1}$. If this ET quenching were associated with a 1:1 complex, the quenching would be described by eq 5. Within this model, the quenching of ^{3}ZnCcP by Fe^{3+}C*c*(horse) must decrease monotonically with increasing concentration of the competitive inhibitor, CuC*c*(*Pm*), because C*c*(*Pm*) binds more tightly to C*c*P than does C*c*(horse); thus, Δk would decrease by more than a factor of 2 over the course of the titration with CuC*c*(*Pm*). Instead, the quenching is slightly enhanced with increasing concentration of the inhibitor CuC*c*(*Pm*). This result transparently shows that the stoichiometry of the [C*c*, C*c*P] complex is not 1:1 but 2:1 or higher. This measurement was complemented with one using CuC*c* in an I_N type of experiment where the ZnC*c*(horse) is titrated by an equimolar mixture of Fe^{3+}C*c*P and the strongly binding inhibitor CuC*c*(*Pm*).

The two titration experiments with the inhibitor CuC*c*(*Pm*) actually were designed to test for "cooperative" ET at the strongly binding domain in the 2:1 C*c*−C*c*P complex (Scheme VI.1). In both experiments, the tight-binding domain on CcP is occupied by a redox-inert CuC*c*(*Pm*), which blocks access to this domain by a redox-active C*c*, either ZnC*c*(horse) or Fe^{3+}C*c*(horse). Thus, the enhanced ET quenching in the presence of inhibitor is inconsistent with the cooperative model of Scheme VI.1 in which ET between C*c*P and a C*c* bound at its strongly binding domain is enhanced when a second C*c* binds at the nonreactive second domain. The experiments instead indicate that the strongly binding domain of C*c*P has low heme−heme ET reactivity. The ET rate constant obtained by fitting the data from the I_N titration ($^2k \sim 1530\ s^{-1}$) is associated with the low-affinity domain within the 2:1 C*c*−C*c*P complex.

The CuC*c* inhibitor also has been used to probe the mechanism of the Fe^{2+}C*c* → ZnC*c*P^+ thermal ET within the [ZnC*c*P^+, Fe^{2+}C*c*] ET intermediate. We

reported previously[116,125] that this reaction displays multiphasic, intracomplex kinetics and provisionally interpreted this in terms of gating by conformational interconversion. The discovery that photoinitiated ET primarily occurs within a 2:1 complex means that the ET intermediate actually has the 2:1 stoichiometry of [ZnC*c*P$^+$, Fe^{2+}C*c*, Fe^{3+}C*c*]. This, in turn, raises the possibility that multiphasic kinetics displayed by this intermediate reflects enhanced electron self-exchange between Fe^{2+}C*c* and Fe^{3+}C*c* on the surface of ZnC*c*P, prior to the reduction of ZnC*c*P$^+$. However, the kinetics of this intermediate is not perturbed significantly when the strong-binding domain is occupied by the CuC*c*(*Pm*) inhibitor, a situation that would eliminate self-exchange ET within the ET intermediate.

The use of CuC*c* as an ET inhibitor thus provides evidence against both the hypothesis of cooperative photoinitiated ET within the 2:1 complex and that of intracomplex self-exchange within the ET intermediate. The simplest kinetic scheme that is consistent with current data involves sequential binding, where the first C*c* binds strongly at a nonreactive domain and the second binds weakly at a reactive one, with the observed ET largely occurring in the 2:1 species.

E. Independent Confirmations of 2:1 Stoichiometry

Although the stoichiometry of binding is still sometimes disputed, the majority of the recent investigations have confirmed and/or extended the occurrence of 2:1 binding as demonstrated by the kinetic measurements just described.

Proton Uptake/Release upon Complex Formation

The existence of two binding domains on C*c*P and the formation of a 2:1 complex was confirmed at μ = 50 mM for an extended range of pH values, 5.5 < pH < 7.75, by potentiometric titration experiments that monitor the uptake and/or release of protons accompanying binding of Fe^{3+}C*c*(yeast iso-1) to Fe^{3+}C*c*P[130] (Figure VI.9). The titration curves obtained by adding the cytochrome to the peroxidase (N titration protocol) show a maximum near $R = 1$. These curves require 2:1 binding and, as the simulations in Figure IV.6 predict, a maximum is observed because the "reactivity parameters", in this case the number of protons taken up during the two stages of binding (q_1 and q_2), have opposite signs. For pH <7, the first stage of binding results in proton release ($q_1 < 0$) and the second binding step results in proton uptake ($q_2 > 0$). The magnitude of the proton uptake for the first binding step (q_1) decreases with increasing pH while that for the second step (q_2) increases (Figure VI.9) until, for pH >7, protons are consumed in the first binding step ($q_1 > 0$) and released in the second step ($q_2 < 0$). The opposing reactivities for the two binding steps at both low and high pH values make the proton uptake experiment exquisitely sensitive in these ranges, while the signals obtained at pH 7 are small and difficult to analyze. Since most kinetic experiments so far have been performed at pH 7, the results from the proton uptake titrations beautifully complement those obtained in kinetic experiments. Together they demonstrate that the 2:1 complex forms over a wide pH range.

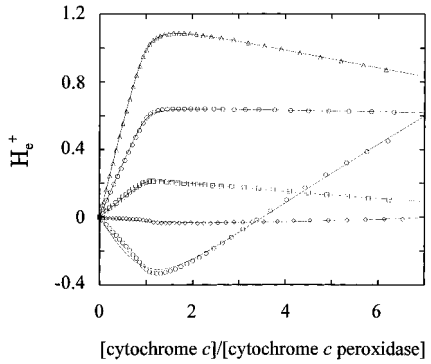

Figure VI.9. Effect of pH on proton release during the titration of C*c*P with Fe^{3+}C*c* (μ= 50 mM, 25 °C, KNO_3): (Δ) pH = 5.51, $P_{initial}$ = 33.9 μM; (○) pH = 5.99, $P_{initial}$ = 34.3 μM; (□) pH = 6.50, $P_{initial}$ = 36.9 μM; (◇) pH = 7.00, $P_{initial}$ = 37.0 μM; and (○, dashed line) pH = 7.75, $P_{initial}$ = 37.2 μM. The lines are unweighted least-squares fits for a model with two binding domains for C*c* per molecule of C*c*P.

Measurements of proton uptake also disclosed that the oxidation state of C*c* influences its interaction with C*c*P,[130] indicating a thermodynamic linkage between ET and binding. At pH 6 and μ = 100 mM, the titration of Fe^{3+}C*c*P with Fe^{2+}C*c* shows the characteristic maximum indicating the presence of a 2:1 complex, whereas results with Fe^{3+}C*c* do not give clear evidence for the existence of a 2:1 complex. The difference arises under these conditions because: (i) proton uptake during the second binding step is greater for Fe^{2+}C*c* than for Fe^{3+}C*c* and (ii) the stoichiometric affinity constant for the first step of binding (K_1) is less for Fe^{2+}C*c* than for Fe^{3+}C*c*. Comparison of the kinetic and proton-uptake measurements over a wider range of pH values will be of keen interest.

Steady-State Kinetics

A reanalysis of the steady-state kinetics[131,132] also shows that two domains and a 2:1 stoichiometry are necessary to interpret the data with C*c*(yeast iso-1) for a broad range of ionic strengths (10−200 mM). With C*c*(horse) a 1:1 stoichiometry seems sufficient, but given that there are two binding domains on C*c*P, even if the ternary complex does not form to a significant extent, the measured stoichiometric rate constant for 1:1 binding must be a weighted average of the parameters for the two domains (eq 14). Consistent with this interpretation, the binding affinities reported in this study are quite comparable to those obtained by heme substitution flash photolysis and by proton-uptake titrations.

Recently Miller et al.[133] studied the stoichiometry of binding through use of a surface-modified C*c*P double mutant in a variety of kinetic experiments, including steady-state measurements, stopped-flow measurements, and photooxidation experiments utilizing Ru-labeled C*c*s. The steady-state measurements support the conclusion that at least two sites (H-mode and Y-mode) exist within the high-affinity domain, and as expected, covalent attachment of the bulky 3-(*N*-maleimidylproprionyl)biocytin (MPB) reagent to the genetically engineered Cys at position 193 (which lies within the interface for the high-affinity domain) lowers the observed reactivity (k_{cat}) and decreases the measured affinity constant (K_m)

to a value that is comparable to that of the low-affinity domain of C*c*P(MI). In contrast to the complex with C*c*P(MI), both K_m and k_{cat} are insensitive to ionic strength, so two stoichiometric binding steps were not discerned even at low ionic strengths. These steady-state measurements with the MPB-modified double mutant were interpreted as ruling out the importance of a second domain. However this is not correct. The observed ionic strength dependence also is consistent with a two-domain model where the measurement has yielded a *stoichiometric* rate constant that reflects the weighted sum of the contributions from both the low-affinity and high-affinity domains. (See section VI.F for further discussion of such a situation.) Alternatively, it may be that binding at the high-affinity domain is completely blocked by MPB, so the steady-state measurements actually monitor a reaction that occurs exclusively at the low-affinity domain.

A key problem with a simple one-domain mechanism for the kinetics of the reaction of C*c*P and C*c* is that the rate of ET from Fe^{2+}C*c* to oxidized states of C*c*P can exceed the rate of release of the product Fe^{3+}C*c*, an impossibility if a second reactant molecule cannot bind until the product molecule dissociates. The contradiction obviously is resolved if reaction can occur at two separate domains. An alternate resolution to the problem, "substrate-assisted product dissociation" was proposed by McLendon.[14] The idea is that a second molecule binds and interacts with the first so as to enhance the rate of dissociation of the first molecule from the principal, tight-binding domain. This is described by eq 27, which requires that both domains be in fast exchange.

$$D^+A^- + A \rightleftharpoons D^+A + A^- \qquad (27)$$

In the present context, the requirement of weak binding by a second C*c* implies the existence of a second interaction domain, and thus the proposal can be viewed as a variant of the two-domain model in which all reaction occurs at the high-affinity domain.

NMR Titrations

The chemical shifts for most of the proton NMR signals detected in a one-dimensional NMR spectrum from equimolar amounts of Fe^{3+}C*c*P(CN^-)[134,135] (or Fe^{3+}C*c*P)[119,136] and Fe^{3+}C*c* are not significantly different from those in the isolated proteins. However, a small subset of the observed signals are perturbed upon binding, and these perturbations have been used to quantitatively describe the binding of C*c*P and C*c*. Because the observed binding-induced shifts are small, efforts to unambiguously detect the 2:1 complex by this technique have been unsuccessful. However, Yi, Erman, and Satterlee[137] found that the dissociation rate constant of 180 s^{-1} obtained from inversion transfer and saturation transfer experiments with either the [Fe^{3+}C*c*P, Fe^{3+}C*c*(yeast iso-1)] complex or the [Fe^{3+}C*c*P(CN^-), Fe^{3+}C*c*(yeast iso-1)] complex is inconsistent with a mechanism for catalytic turnover involving sequential oxidation of two molecules of Fe^{2+}C*c* at a single C*c* binding domain. Rather, these NMR experiments support either a two-domain binding mechanism or the substrate-assisted-dissociation variant of the two-domain model. In either case, the concentrations of C*c*P and C*c* employed for NMR experiments should produce appreciable levels of 2:1 complex, so the measured dissociation rate constant is likely a composite of the dissociation rate constants for the individual domains.

Fluorescence Line-Narrowing Spectroscopy

Because ET reactions in the [C*c*P, C*c*] complex involve long-range processes, spectroscopic techniques that predominantly monitor the redox-active chromophores often are unperturbed by complexation. For example, resonance Raman measurements showed no evidence of changes in C*c* upon complexation with C*c*P.[138,139] Fluorescence line-narrowing (FLN) studies[140] at 4 K showed that binding of C*c* to meso-porphyrin-substituted C*c*P induces changes in the relative distribution of luminescent components. Furthermore, the distribution of the components for a sample containing equimolar amounts of C*c*P and C*c* and for a second sample containing excess C*c* are different. Such results is consistent with formation of a 2:1 complex.

F. Kinetic and Physical Characterization of Site-Specific Mutants of C*c*P

Site-directed mutagenesis is being used to identify the structural elements that are responsible for the stability of the higher oxidation states of C*c*P[141−146] and for promoting heterolytic fission of the peroxide O−O bond,[147] to probe the details of the mechanism in which the two distinct redox centers of ES are reduced by Fe^{2+}C*c* to the resting state,[91,148−153] and to identify the amino acid residues that comprise the two surface binding domains.[107,108,154−156] We discuss only those mutations that address issues of binding and reactivity. Studies with mutants of C*c* that affect its interaction with C*c*P have been reviewed thoroughly by Mauk,[157] so we focus here on mutants of C*c*P.

Trp 191

This residue is the radical site in H_2O_2-oxidized intermediate, compound ES, and in C*c*P-II_r. Thus, substitution of Trp 191 is an obvious strategy for addressing the mechanism of heme reduction in C*c*P. The indole ring of Trp 191 lies parallel to and in van der Waals contact with the proximal ligand His 175. Extensive kinetic and physical characterization studies have been reported for the Phe 191 mutant, and to a lesser extent for the Gly 191 and Gln 191 mutants. Replacement of Trp 191 with Gly enables exogenous cations, such as imidazolium, to bind in the space vacated by Trp 191.[158] Resonance Raman studies[141] with the resting state of the Phe 191 mutant indicate that the heme is predominantly pentacoordinate and high-spin, like the native protein. Optical studies indicate that reaction of this mutant with H_2O_2 leads to oxidation of the heme to the ferryl state but that the oxidized product has been significantly destabilized relative to C*c*P-I(MI). A stable radical not associated with Phe 191 was observed by EPR,[159,160] suggesting that there is an alternative amino acid site capable of storing oxidizing equivalents. Significant changes in the kinetics[161] for the initial formation of the oxidized inter-

mediate and its subsequent reduction by ET from Fe^{2+}C*c* were observed for the Trp 191 → Phe mutant. The absence of heme−heme ET when Trp 191 is mutated is fully consistent with a picture where heme−heme ET is dominated by reactions at the low-affinity domain and thus fully consistent with the heme substitution measurements described above.

Proximal Side Mutation Sites

Examination of the X-ray structure of C*c*P[93] shows that Trp 191 is connected to the heme site by a hydrogen-bond network that includes Asp 235 and the proximal ligand (His 175), with Asp 235 forming hydrogen-bonds to both Trp 191 and His 175. This network is expected to modulate the electronic properties of the heme, to stabilize the indole group of Trp 191, and to modify the redox potentials of the heme and the Trp radical. The Asp−His interaction is believed to deprotonate the His to form an imidazolate ligand, which leads to an increase in the metal−ligand bond strength. In addition, Asp 235 provides a conduit for mediating coupling between the Trp 191 radical and the heme.

Goodin and McRae[162] have shown that the C*c*P-(D235E) mutant retains many of the coordination and functional properties of wild-type C*c*P, despite significant structural changes. The H-helix (residues 233−242) is sufficiently flexible and reorients slightly to accommodate the additional CH_2 group of Glu 235, without disrupting the hydrogen-bonding network. Although there is a small rotation of His 175, the overall position of the carboxylate group is nearly unchanged. In contrast, ET reactivity is greatly changed in the C*c*P(D235N)[163] and C*c*P(D235A)[153] mutants. X-ray analysis[162] shows that replacement of Asp by either Asn or Ala disrupts both of these hydrogen bonds and that the indole side chain of Trp 191 has flipped over to form a new hydrogen bond between the indole NH and the backbone carbonyl of Leu 177.[164] Although the heme can be oxidized to the ferryl state, both of these mutants show negligible enzymatic activity, and no photoinitiated ET reaction was observed with Ru27-C*c*(horse).[163]

By comparing the X-ray structure of C*c*P to those of other peroxidases, in particular that of ascorbate peroxidase (APX),[165] Bonagura et al.[166] found a cation-binding site located 8 Å from the proximal Trp in APX that is absent in C*c*P. The absence of this cation-binding site is believed to be one reason why a stable Trp radical is formed in C*c*P but is absent in APX. To test the importance of this cation-domain in controlling whether oxidizing equivalents can be stored on the proximal Trp, site-directed mutagenesis was used to create a cation-binding site in C*c*P.[166] Spectroscopic characterization of this mutant showed that a stable Trp radical does not form but that the oxidizing equivalent resides instead on the porphryin ring. The steady-state activity for the oxidation of Fe^{2+}C*c* is significantly decreased for this mutant, confirming the hypothesis that long-range electrostatic effects destabilize the Trp radical and lower the redox activity of C*c*P.

Surface Mutation Sites on CcP

Kinetic studies with the wild-type yeast C*c*P confirm the occurrence of 2:1 stoichiometry for [C*c*, C*c*P] complexes and therefore the existence of two distinct binding domains with different reactivities, but the physiological significance of the domain identified by crystallography and the location of the well-established "second" domain on C*c*P remain fundamental unanswered questions. The most promising method for experimentally locating these recognition domains couples kinetic studies with site-directed mutagenesis. The initial set of target surface sites was inspired by the Poulos−Kraut electrostatic model[98] and subsequently by the crystal structure,[99] both of which focus on the high-affinity domain. The residues suggested by the Poulos−Kraut model include Asp 34, Asp 37, Asp 79, Gln 86, Asn 87, and Asp 216, whereas the set of C*c*P surface residues specified from the [C*c*P, C*c*(horse)] crystal structure include (i) Ala 193 and Ala 194, which predominantly interact with the heme of C*c*; (ii) Glu 35, Asn 38, and Glu 290, which form H-bonds with surface Lys of C*c*; and (iii) Tyr 39 and Asp 34, which are involved in van der Waals interactions with the C*c* surface. Additional residues that are potentially important in stabilizing the [C*c*P, C*c*(yeast iso-1)] complex include Arg 31, Gln 120, and Val 197, which are in van der Waals contact with the surface of C*c*. Although the Brownian dynamics calculations of Northrup[109−112] suggest that the second domain lies in the vicinity of Asp 148, the location of the well-established "second" domain remains a challenge for future studies.

Miller et al.[155] have used stopped-flow experiments and flash photolysis to study a set of mutants where individual carboxylate side chains have been converted to amides; these include C*c*P(E32Q), C*c*P-(D34N), C*c*P(E35Q), C*c*P(E290N), and C*c*P(E291Q). Residues 32 and 291 are remote from the high-affinity domain, and consequently, the kinetics for the C*c*P(E32Q) and C*c*P(E291Q) mutants is similar to that of the native protein. On the other hand, when mutations were made at positions that lie within the interface identified by X-ray diffraction (34, 35, and 290), the reactivity is decreased relative to that of the native protein. Although the decreased reactivity could represent either a perturbation in binding affinity and/or ET reactivity, the perturbation in the kinetics indicates that these residues may be functionally important.

Corin et al.[123,156] have prepared a set of charge-reversal mutants where one surface Asp has been converted to Lys at positions 37, 79, or 217. The kinetic behavior of the C*c*P(D217K) mutant was similar to that of the native protein, whereas the instability of the ES state of the C*c*P(D79K) mutant prevented a complete kinetic characterization of this mutant. The C*c*P(D37K) mutant showed remarkably different kinetics from the native CcP. This is not unexpected, since the Poulos−Kraut model recognized Asp 37 as one of the interface residues involved in charge−pair interactions with surface Lys on Cc, and in the crystal structure Asp 37 lies proximal to the recognition site for Fe^{3+}C*c*(horse).

As an illustration of how kinetic studies with point-mutations can be used to begin to locate the strong-binding domain, we now discuss photoinduced ET between ZnC*c* and the charge-reversal C*c*P mutant in which the negatively charged Asp 37 residue is

replaced by a positively charged lysine residue. The C*c*P(D37K) mutant behaves very differently from C*c*P(WT) in binding and heme−heme ET.[167] In the I_R titration of Fe^{3+}C*c*P(D37K) by ZnC*c*, Δk decreases monotonically as ZnC*c*(horse) increases, in contrast to the I_R titration of wild-type C*c*P by ZnC*c* (Figure VI.7). The behavior of the mutant is perfectly described by a 1:1 binding isotherm with an intermediate value for the *stoichiometric* binding constant ($K_1 \sim 10^4$ M^{-1}), indicating that the amount of 2:1 [C*c*,C*c*P] complex in solution is negligible. The significant decrease in K_1 from 8.5×10^5 M^{-1} for C*c*P(WT) to 10^4 M^{-1} for C*c*P(D37K) clearly indicates that the surface area identified by Pelletier and Kraut is the strong binding domain or at least part of it. Although the *stoichiometric* constant for binding of C*c* is greatly decreased by the mutation of Asp 37 to Lys in C*c*P, the *stoichiometric* intracomplex ET rate constant (k_1) is greatly increased: k_1(WT) = 40 s^{-1}; k_1(D37K) = 3900 s^{-1}. Furthermore, the ionic strength dependence of the intracomplex ET rate constant (k_1) within the 1:1 complex differs sharply for C*c*P(WT) and C*c*P(D37K): k_1 decreases for C*c*P(D37K) as the ionic strength increases, whereas it increases for C*c*P(WT).

This kinetic behavior can be understood easily by recognizing that C*c* binds with widely different reactivities at two different domains on C*c*P and that the mutation of Asp 37 to Lys differentially affects the C*c*-binding affinities at these two binding domains. Since residue 37 is proximal to the high-affinity domain, substitution of the negatively charged Asp 37 residue with a positively charged Lys greatly weakens the C*c*-binding affinity at the high-affinity domain (reduces K_{10}) because of the net loss of two negative charges on C*c*P along with the introduction of a repulsive interaction between the now positively charged Lys 37 of C*c*P(D37K) and the positively charged lysine residues of C*c* located at the exposed edge of its heme. According to eqs 11 and 12, a mutation that lowers the stoichiometric binding constant K_1 also lowers the stoichiometric binding constant K_2, so that only the complexes with *1:1 stoichiometries* contribute to the quenching of ^{3}ZnC*c* by Fe^{3+}C*c*P(D37K) under our experimental condition. However, this does not mean that only one domain is involved! The increase in k_1 from 40 s^{-1} for C*c*P(WT) to 3900 s^{-1} for C*c*P(D37K) can be understood in terms of eq 8, which shows that even for a 1:1 binding stoichiometry, the stoichiometric rate constant k_1 is a weighted average of the two domain rate constants, weighted according to the relative populations of the two conformers of the 1:1 complex. The mutational weakening of the binding at the high-affinity domain effectively acts to *increase* 1:1 binding at the highly reactive second domain by ca. 2 orders of magnitude. The result, described by eq 8, is that the *stoichiometric* rate constant (k_1) is increased significantly, even though the *domain* rate constants are not affected by the mutation.

The ionic strength dependence of k_1 for the [ZnC*c*, Fe^{3+}C*c*P(D37K)] complex likewise can be explained by considering the relationships between the measured stoichiometric parameters and the derived domain constants (eqs 5 and 8). Because of a difference in the ionic strength dependence of the binding affinities, K_{10} and K_{20}, the fraction of the heme-et-inactive 1:1 complex (^{1}ES) increases as the ionic strength increases, resulting in the decrease in k_1 from 3900 to 1000 s^{-1}.

G. Surface Coupling Maps and Electrostatic Maps of the [C*c*P,C*c*] Complex

We now compare the pathway surface coupling maps and the surface electrostatics maps of the [C*c*, C*c*P] reaction pair. Our goal is to use theoretical methods to propose logical choices for the experimentally determined weak-binding/fast heme−heme ET and tight-binding/slow heme−heme ET domains on C*c*P. Our method of reconciling the information about docking geometry and electronic coupling is to seek correspondence between the surface coupling maps and the electrostatic maps. In order to identify the loci on the C*c* and C*c*P surfaces that are strongly coupled to the hemes, a pathway global coupling calculation was performed (section V.B). Figure VI.10a−d shows the surface coupling maps for Fe^{3+}C*c*P and Fe^{3+}C*c*(horse). The Trp 191 indole ring is delocalized when treated as the ET-active site in the pathway coupling calculation of C*c*P. Asymmetry of the Trp wave function on the indole ring and complications arising from coupled deprotonation dynamics are beyond the scope of this simple analysis. We analyzed the protein electrostatics using the DelPhi program (section V.C). Figure VI.10e,f shows the electrostatic maps for both proteins. Both the electrostatic studies and the surface coupling studies were performed on the isolated proteins (investigations on docked structures are in progress).

We have identified a crescent-shaped region on the surface of C*c*P that exhibits relatively strong electronic coupling to the heme (Figure VI.10c,d). Within this region are areas that are electrostatically complementary to the C*c* surface (Figure VI.10e,f). One complementary area on the C*c*P surface falls between Tyr 39 and Asp 217. This area comprises a single binding domain with two overlapping binding sites (sites 1and 2) or a continuum of binding sites. A second distinct complementary area lies near Asp 148. This area comprises a second binding domain with a single site (site 3). Pathway couplings to Trp 191 are strongest for site 1, intermediate for site 2, and weakest for site 3. In the region surrounding sites 2 and 3 on the C*c*P surface, strong coupling and strong negative potentials coincide. Because our initial studies have focused on the individual process, it is difficult to quantitatively differentiate the electronic coupling strengths and electrostatic contributions across the three interaction surfaces.

Figure VI.11 shows a schematic view of the proposed docking regions on the C*c*P surface. Site 1 (labeled as Tyr 39) has the strongest concentration of surface charges and is the only site that was detected in the 1:1 [C*c*P, C*c*] crystalline complex.[99] Other amino acid residues in this region are Asn 38 and Glu 290. Site 2 is in the region of the Poulos and Kraut hypothetical complex obtained by optimizing the intracomplex hydrogen bonding interactions.[93] Other nearby amino acids are Asp 37, Asp 34, and Asp 79. Site 1 and site 2 clearly overlap and thus comprise a single domain with two overlapping sites (or a continuum of binding sites). Site 3, which

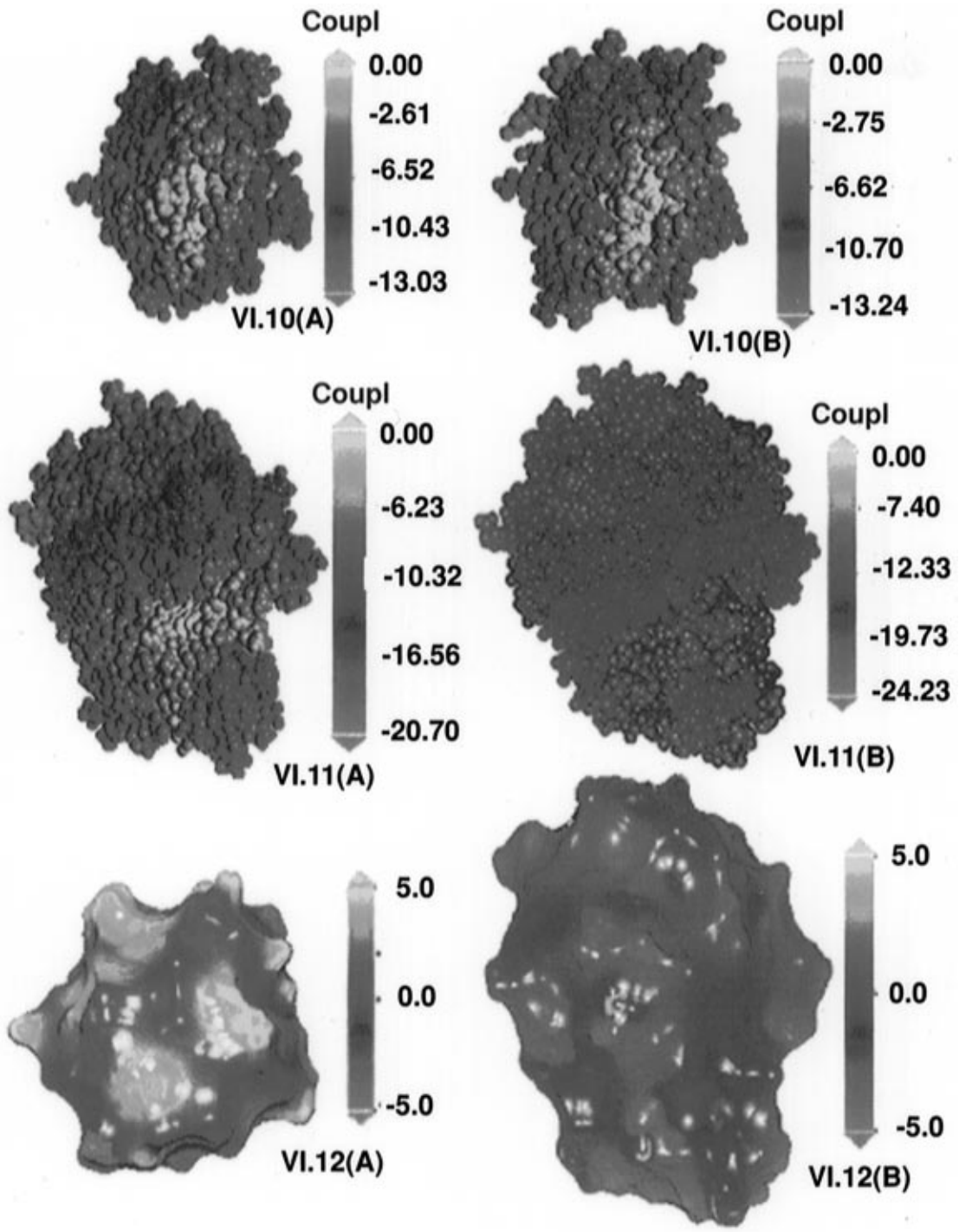

Figure VI.10. Pathway couplings (eq 20) from the heme to the surface atoms in (a, upper left) Fe^{3+}C*c*(horse) and (b, upper right) Fe^{3+}C*c*(yeast iso-1). The coupling scale shows the logarithm of the pathway coupling value $\prod_i \epsilon_i$. Note the strong coupling surface associated with the heme crevice. Pathway couplings are shown from (c, middle left) the heme p-electron ring and (d, middle right) the Trp 191 side chain of C*c*P to the protein surface. Note the crescent-shaped strong coupling surface. Electrostatic potential surfaces computed with the program Del Phi[79] for (e, lower left) the Fe^{3+}C*c*(horse) encounter surface and (f, lower right) the Fe^{3+}C*c*P encounter surface. The scale shows electrostatic potential in units of k_BT/e, with $T = 25$ °C. There is complementarity between the potentials, strong coupling pathways, and encounter surface shapes between C*c*P residues Thr 39 and Asp 217. A third complementary site on the C*c*P surface lies near Asp 148. These potential docking and ET regions are in the same regions as those proposed by Northrup and co-workers.[109,110]

meets the docking criteria for ET, based on Brownian dynamics simulation, was described by Northrup and co-workers[109,110] and is centered near Asp 148. Other participating residues include Gln 152, Phe 140, and Leu 221. The residue located between these two domains is Asp 217. The surface coupling maps for C*c*P are qualitatively similar for the analysis of pathways into both the heme and Trp 191.

The encounter surface for Fe^{3+}C*c*(horse) (generated by tracing with a 5 Å radius probe) is shown in Figure VI.10e,f. Here the front view of the encounter surface is shown along the Fe to heme C4C direction. The color of the encounter surface ranges from blue to red for electrostatic potential values of $-5k_BT$ to $5k_BT$, respectively. The amino acid region of strongest positive potential includes Lys 4, 5, 11, 13, 72, 73,

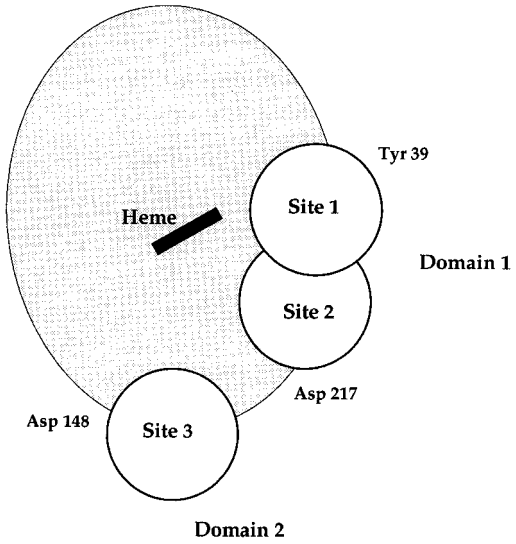

Figure VI.11. Schematic representation of the low-energy binding sites associated with [C*c*, C*c*P] functional docking. The regions were determined on the basis of (1) strong coupling pathways to the redox centers in the individual proteins, (2) electrostatic complementarity, and (3) rough encounter surface shape complementarity.

86, and 89. Regions on the C*c* surface (Figure VI.10a,b) that are most strongly coupled to the heme lie around the heme crevice and coincide with regions on the electrostatic maps where the electrostatic potential is largely positive (Figure VI.10e,f). Tiede[74] computed electrostatic maps for a number of cytochromes *c* with the program DelPhi.[79] Our calculations are consistent with those, and with the Brownian dynamics calculations of Northrup and coworkers.[109]

We have mentioned the challenge of understanding single pathway vs pathway "tube" coupling mechanisms. The propensity toward one mechanism or another in unimolecular reactions need not be the same as in bimolecular reactions. That is, interprotein coupling interactions at the protein−protein interface are somewhat different in magnitude and number from the kinds of electronic interactions within each protein. As such, it remains to be seen whether the protein−protein interface presents single pathway, pathway "tube", or average medium effects and how substantially they perturb the nature of pathways within the individual reaction partners. A particularly important application of multipathway Green function techniques will be to probe the nature of multipathway interferences at protein−protein interfaces.

VII. Discussion

This review has had several central purposes. Section III discusses the critical connection between the binding and kinetic parameters that are obtained from experimental measurements and the microscopic constants that are the ultimate goal of those measurements. In part, this represents the rebottling of old wine in new bottles, as these considerations have been thoroughly explored in the context of ligand binding,[35−37] but their extension to the definition of stoichiometric rate constants is new. The whole issue is not well-embedded into the literature of interprotein electron transfer. In section IV we present an expanded view of titration experiments as generating four-dimensional data sets, with quenching measurements yielding not curves but 2-D surfaces. This in turn naturally leads to the expansion of quenching protocols to include the four types of titration listed in Table IV.1. As reviewed in section VI, the four types of titration experiments (Table IV.1) together demonstrate that (i) C*c* reacts at two distinct and nonexclusive surface domains of C*c*P; (ii) two molecules of C*c* can bind simultaneously to C*c*P; (iii) the ternary complex is more reactive than the binary complex for the heme−heme ET reaction; and (iv) the use of CuC*c* as inhibitor suggests that these results are to be interpreted as meaning that one domain has a high affinity for C*c* but a low reactivity for the heme−heme ET reaction, while the low-affinity domain is highly reactive in heme−heme ET. Taken together, these results suggest a mechanism where ET at the strongly binding domain leads to reduction of the Trp radical and ET at the weak binding domain is optimized for reduction of the ferryl-heme.

It has been generally accepted that the high-affinity domain on the surface of C*c*P is in the general vicinity of the binding domain first identified by Poulos and Kraut[98] or perhaps at the different but overlapping site detected in the cocrystal,[99] but with the proviso that multiple binding orientations must exist, as evidenced by instances of gated electron transfer. Section V extends the "pathways" model for calculating ET rate factors to protein−protein ET via the concept of functional docking and discusses the use of classical electrostatics calculations to characterize the encounter surface. As to the location of the second domain, the Brownian dynamics calculation of Northrup and Thomasson suggests that the low-affinity domain may be found in the vicinity of Asp 217 (Figure VI.1).

We performed three kinds of theoretical analyses on the C*c*/C*c*P system. The first is a surface coupling tunneling pathway analysis. This calculation approximates the coupling between the protein redox centers and the protein surface. Strongly coupled regions of C*c* appear near the heme crevice, while strongly coupled regions around the C*c*P appear in a broader, crescent-shaped region. Strongly coupled surface amino acids in this crescent couple to the heme edge. A second strategy of analysis, functional docking, suggests that the interactions between surface amino acids of the two proteins in these two strong pathway patches, taken together with the pathway couplings to each redox center from its corresponding surface patch, set an upper bound on the ET rate. A third calculation was performed in order to further refine this analysis. Electrostatic encounter surface potentials were computed for two proteins to examine electrostatic complementarity that might exist in the region of relevance suggested in the functional docking analysis. Two domains were found with similar pathway couplings to the heme and with complementary electrostatics. The domains differ somewhat in their radii of curvature. Also, the first domain is more strongly coupled to the Trp 191 than is the second domain. This analysis

has not sought out alternative domains with considerably weaker electronic interactions between the two redox centers, although many such docking geometries surely exist.

Support for the definitive finding that heme−heme ET is more efficient in the 2:1 complex than in the 1:1 complex and the resulting suggestion that the binding domain identified by the X-ray structure may be optimized for reactions with the Trp^+ radical site, but may not be the physiologically active site for heme-centered reactions, in fact is given by flash photolysis studies of ET between ruthenium-labeled C*c*s and compound ES.[33,34] These studies indicate that C*c* bound at the high-affinity domain reduces the Trp radical, not the heme site, so that the product of the first reduction step of ES is C*c*P-II_h, in which the one oxidizing equivalent is on the heme. It was further suggested that this is followed by rapid intramolecular ET between the oxidized heme and the Trp to generate C*c*P-II_r (eq 24).

$$ES \rightleftarrows CcP\text{-}II_h \rightleftarrows CcP\text{-}II_r \qquad (24)$$

Return to the resting state then involves reduction of the Trp radical in C*c*P-II_r. In this mechanism, ferryl-heme reduction is not the result of direct transfer to the heme but of a two-step process that involves the Trp. From this the authors of this study concluded that the heme-centered reduction and the Trp-centered reduction proceed along a common "pathway" and that both oxidizing equivalents *necessarily* are transferred to the C*c* through a common binding domain. However, a number of considerations show this conclusion to be invalid. Firstly, the stopped-flow studies and photoinitiated ET studies with Ru-labeled C*c*s are carried out under highly *nonphysiological* conditions in which the concentration of Fe^{2+}C*c* is comparable to or less than that of compound ES. But, this assures that binding occurs predominantly at the high-affinity domain and precludes examination of the weakly binding one! In other words, while the experiments elegantly demonstrate that heme reduction at the high-affinity domain can regenerate the resting state in a two-stage process, from C*c* to Trp to ferryl-heme, the experimental conditions in fact eliminate the possibility of detecting *direct* heme−heme ET from a cytochrome that binds and reacts at the low-affinity domain. Thus, the "conclusion" that heme reduction occurs only by reaction at a single domain is invalid and rather is a *consequence* of the measurement technique. One should also recall that, as noted above, intraprotein ET between the ferryl-heme and the Trp of C*c*P is a poorly understood process that under some circumstances can be far slower than the measured rate constant for reduction by Fe^{2+}C*c*.[87,88,92,148,168,169]

The heme substitution titration procedures, in contrast, are successful in characterizing the two-domain binding and in demonstrating direct heme−heme reactivity at the more weakly binding domain. This is true in part because metal substitution simplifies the reaction mechanism, looking only at the heme−heme process, but also because the quenching measurements more accurately mimic the physiological situation in which C*c* is in abundance, which facilitates the operation of *parallel* reaction processes (and pathways), one in which the C*c*P ferryl-heme is directly reduced by Fe^{2+}C*c* bound at the low-affinity domain. In fact, the heme substitution measurements described above show that Fe^{2+}C*c* bound at the high-affinity domain does not undergo heme−heme ET when the Trp radical is not oxidized and that this does *not* eliminate heme-centered ET to Fe^{2+}C*c*, thereby disproving the notion that there is but one "portal" for the entry of reducing equivalents into C*c*P-I. Indeed, the rate constant for the reduction of Zn*Cc*P^+ by Fe^{2+}C*c* is quite similar to the rate constant reported for the heme-centered reduction of C*c*P-II,[133] and thus, metal substitution *demonstrates* the presence of an ET pathway to the C*c*P heme that does not involve transient oxidation of Trp 191.

The conclusions from the work described are (i) reduction of the Trp radical occurs preferentially at the high-affinity domain; (ii) under conditions where equilibration of C*c*P-II_h and C*c*P-II_r is slow compared to the direct heme−heme reduction at the low-affinity domain, heme reduction also occurs preferentially at the high-affinity domain; (iii) under conditions where equilibration is rapid, heme reduction by Fe^{2+}C*c* occurs independently at both domains, through a two-step process at the high-affinity domain but directly at the low-affinity domain; (iv) functional docking calculations suggest a possible (and testable) identity for the low-affinity domain. It also seems probable that under conditions where C*c*P-II_h and C*c*P-II_r equilibriate that the Trp radical is reduced through a two-step process at the low-affinity domain. One might surmise that misplaced emphasis on reactivity at a single domain in part may be inspired by inappropriate use of the X-ray structure of the 1:1 complex. Whereas, crystallization selects the least soluble species from a solution, this need not correspond to the most active species and certainly need not be the only reactive one. The reasonable conclusion from this review itself is that new methods of approaching ET in protein−protein complexes have opened a new era in this enterprise.

Acknowledgments

This work has been supported by the NIH through Grants HL13531 (B.M.H.) and GM48043 (D.N.B., J.N.O.). We thank Jeff Regan and Paul Beroza for their assistance in the preparation of Figures V.2 and V.3, respectively.

References

(1) Marcus, R. A.; Sutin, N. *Biochim. Biophys. Acta* **1985**, *811*, 265−322.
(2) Deisenhofer, J.; Norris, J. R. *The Photosynthetic Reaction Center*, Academic Press: San Diego, 1993; Vol. I.
(3) Wasielewski, M. R. *Chem. Rev.* **1992**, *92*, 435−461.
(4) Closs, G. L.; Miller, J. R. *Science* **1988**, *240*, 440−447.
(5) Winkler, J. R.; Gray, H. B. *Chem. Rev.* **1992**, *92*, 369−379.
(6) McLendon, G.; Hake, R. *Chem. Rev.* **1992**, *92*, 481−490.
(7) Hoffman, B. M.; Natan, M. J.; Nocek, J. M.; Wallin, S. A. *Struct. Bonding* **1991**, *75*, 85−108.
(8) Kostíc, N. M. *Metal Ions Biol. Syst.* **1991**, *27*, 129.
(9) Beratan, D. N.; Onuchic, J. N. In *Electron Transfer in Inorganic, Organic, and Biological Systems*; Bolton, J. R., Mataga, N., McLendon, G., Eds.; Advances in Chemistry 228; American Chemical Society: Washington, DC, 1991; pp 71−90.
(10) Natan, M. J.; Baxter, W. W.; Kuila, D.; Gingrich, D. J.; Martin, G. S.; Hoffman, B. M. In *Electron Transfer in Inorganic, Organic, and Biological Systems*; Bolton, J. R., Mataga, N., McLendon, G., Eds.; Advances in Chemistry 228; American Chemical Society: Washington, D. C., 1991; pp 201−213.

(11) Therien, M. J.; Chang, J.; Raphael, A. L.; Bowler, B. E.; Gray, H. B. *Struct. Bonding* **1991**, *75*, 109−129.
(12) Bowler, B. E.; Raphael, A. L.; Gray, H. B. *Prog. Inorg. Chem.: Bioinorg. Chem.* **1990**, *38*, 259−322.
(13) Durham, B.; Pan, L. P.; Hahm, S.; Long, J.; Millett, F. In *Electron Transfer in Biology and the Solid State*; American Chemical Society: 1990; pp 181−193.
(14) McLendon, G. *Struct. Bonding* **1991**, *75*, 159−174.
(15) Hoffman, B. M.; Ratner, M. R. *J. Am. Chem. Soc.* **1987**, *109*, 6237−6243.
(16) Berg, O. G.; von Hippel, P. H. *Annu. Rev. Biophys. Biophys. Chem.* **1985**, *14*, 131−160.
(17) Millett, F.; Miller, M. A.; Geren, L.; Durham, B. *J. Bioenerg. Biomemb.* **1995**, *27*, 341−351.
(18) Stemp, E. D. A.; Hoffman, B. M. *Biochemistry* **1993**, *32*, 10848−10865.
(19) Zhou, J. S.; Hoffman, B. M. *J. Am. Chem. Soc.* **1993**, *115*, 11008−11009.
(20) Zhou, J. S.; Kostíc, N. M. *J. Am. Chem. Soc.* **1993**, *115*, 10796−10804.
(21) Qin, L.; Kostíc, N. M. *Biochemistry* **1994**, *55*, 12392−12399.
(22) Brooks, H. B.; Davidson, V. L. *Biochem. J.* **1993**, *294*, 211−213.
(23) McGourty, J. L.; Blough, N. V.; Hoffman, B. M. *J. Am. Chem. Soc.* **1983**, *105*, 4470−4472.
(24) Winkler, J. R.; Nocera, D. G.; Yocom, K. M.; Bordignon, E.; Gray, H. B. *J. Am. Chem. Soc.* **1982**, *104*, 5798−5800.
(25) Simolo, K. P.; McLendon, G. L.; Mauk, M. R.; Mauk, A. G. *J. Am. Chem. Soc.* **1984**, *106*, 5012−5013.
(26) McLendon, G. L.; Winkler, J. R.; Nocera, D. G.; Mauk, M. R.; Mauk, A. G.; Gray, H. B. *J. Am. Chem. Soc.* **1985**, *107*, 739−740.
(27) Liang, N.; Kang, C. H.; Ho, P. S.; Margoliash, E.; Hoffman, B. M. *J. Am. Chem. Soc.* **1986**, *108*, 4665−4666.
(28) Ho, P. S.; Sutoris, C.; Liang, N.; Margoliash, E.; Hoffman, B. M. *J. Am. Chem. Soc.* **1985**, *107*, 1070−1071.
(29) Kuila, D.; Natan, M. J.; Rogers, P.; Gingrich, D. J.; Baxter, W. W.; Arnone, A.; Hoffman, B. M. *J. Am. Chem. Soc.* **1991**, *113*, 6520−6526.
(30) Moore, G. R.; Williams, R. J. P.; Chien, J. C. W.; Dickinson, L. C. *J. Inorg. Biochem.* **1980**, *12*, 1−15.
(31) Anni, H.; Vanderkooi, J. M.; Mayne, L. *Biochemistry* **1995**, *34*, 5744−5753.
(32) Findlay, M. C.; Dickinson, L. C.; Chien, J. C. W. *J. Am. Chem. Soc.* **1977**, *99*, 5168−5173.
(33) Geren, L.; Hahm, S.; Durham, B.; Millett, F. *Biochemistry* **1991**, *30*, 9450−9457.
(34) Hahm, S.; Durham, B.; Millett, F. *Biochemistry* **1992**, *31*, 3472−3477.
(35) Klotz, I. M. *Introduction to Biomolecular Energetics, Including Ligand-Receptor Interactions*; Academic Press: New York, 1986.
(36) Van Holde, K. E. *Physical Biochemistry*, 2nd ed.; Prentice-Hall: Englewood Cliffs, 1985.
(37) Strickland, S.; Palmer, G.; Massey, V. *J. Biol. Chem.* **1975**, *250*, 4048−4052.
(38) Demas, J. N. *Excited State Lifetime Measurements*; Academic Press: New York, 1983.
(39) Turro, N. J. *Modern Molecular Photochemistry*; Benjamin/Cummings Publishing Co.: Menlo Park, CA, 1978.
(40) Stern, O.; Volmer, M. *Physik. Z.* **1919**, *20*, 183−188.
(41) Hoffman, B. M.; Ratner, M. A.; Wallin, S. A. In *Advances in Chemistry Series*; Johnson, M. K., King, R. B., Kurtz, D. M., Jr., Kutal, C., Norton, M. L., Scott, R. A., Eds.; American Chemical Society: Washington, D. C., 1990; pp 125−146.
(42) Bendall, D. S. *Protein Electron Transfer*; BIOS Scientific Publishers: Oxford, 1996.
(43) Beratan, D. N.; Onuchic, J. N. *Photosynth. Res.* **1989**, *22*, 173−186.
(44) Onuchic, J. N.; Beratan, D. N. *J. Chem. Phys.* **1990**, *92*, 722−733.
(45) Beratan, D. N.; Onuchic, J. N.; Betts, J. N.; Bowler, B. E.; Gray, H. B. *J. Am. Chem. Soc.* **1990**, *112*, 7915−7921.
(46) Beratan, D. N.; Betts, J. N.; Onuchic, J. N. *Science* **1991**, *252*, 1285−1288.
(47) Beratan, D. N.; Betts, J. N.; Onuchic, J. N. *J. Phys. Chem.* **1992**, *96*, 2852−2855.
(48) Onuchic, J. N.; Beratan, D. N.; Winkler, J. R.; Gray, H. B. *Annu. Rev. Biophys. Biomol. Struct.* **1992**, *21*, 349−377.
(49) Beratan, D. N.; Onuchic, J. N. In *Protein Electron Transfer*; Bendall, D. S., Ed.; BIOS Scientific Publishers: Oxford, 1996.
(50) Regan, J. J.; Risser, S. M.; Beratan, D. N.; Onuchic, J. N. *J. Phys. Chem.* **1993**, *97*, 13083−13088.
(51) Skourtis, S. S.; Regan, J. J.; Onuchic, J. N. *J. Phys. Chem.* **1994**, *98*, 3379−3388.
(52) Regan, J. J.; DiBilio, A. J.; Langen, R.; Skov, L. K.; Winkler, J. R.; Gray, H. B.; Onuchic, J. N. *Chem. Biol.* **1995**, *2*, 489−496.
(53) Skourtis, S. S.; Onuchic, J. J.; Beratan, D. N. *Inorg. Chim. Acta* **1996**, *243*, 167−175.
(54) Priyadarshy, S.; Skourtis, S. S.; Risser, S. M.; Beratan, D. N. *J. Chem. Phys.* **1996**, *104*, 9473−9481.
(55) Curry, W. B.; Grabe, M. D.; Kurnikov, I. V.; Skourtis, S. S.; Beratan, D. N.; Regan, J. J.; Aquino, A. J. A.; Beroza, P.; Onuchic, J. N. *J. Bioenerg. Biomemb.* **1995**, *27*, 285−293.
(56) Gruschus, J. M.; Kuki, A. *J. Phys. Chem.* **1993**, *97*, 5581−5593.
(57) Siddarth, P.; Marcus, R. A. *J. Phys. Chem.* **1993**, *97*, 2400−2403.
(58) Stuchebrukov, A.; Marcus, R. A. *Inorg. Chim. Acta* **1996**, *243*, 271−282.
(59) Okada, A.; Kakitani, T.; Inoue, J. *J. Phys. Chem.* **1995**, *99*, 2946−2948.
(60) Balabin, I. A.; Onuchic, J. N. *J. Phys. Chem.* **1996**, *100*, 11573−11580.
(61) Kurnikov, I. V.; Beratan, D. N. *J. Chem. Phys.* **1996**, in press.
(62) Casimiro, D. R.; Richards, J. H.; Winkler, J. R.; Gray, H. B. *J. Phys. Chem.* **1993**, *97*, 13073−13077.
(63) Wuttke, D. S.; Bjerum, M. J.; Winkler, J. R.; Gray, H. B. *Science* **1992**, *256*, 1007−1009.
(64) Wuttke, D. S.; Bjerum, M. J.; Chang, I.-J.; Winkler, J. R.; Gray, H. B. *Biochim. Biophys. Acta* **1992**, *1101*, 168−170.
(65) Langen, R.; Chang, I.-J.; Germanas, J. P.; Richards, J. H.; Winkler, J. R.; Gray, H. B. *Science* **1995**, *268*, 1733−1735.
(66) Karpischin, T. B.; Grinstaff, M.; Komar-Panicucci, S.; McLendon, G.; Gray, H. B. *Structure* **1994**, *94*, 415−422.
(67) Moreira, I.; Sun, J.; Cho, M. O.; Wishart, J. F.; Isied, S. S. *J. Am. Chem. Soc.* **1994**, *116*, 8396−8397.
(68) Chen, L.; Durley, R. C. E.; Matthews, F. S.; Davidson, V. L. *Science* **1994**, *264*, 86−90.
(69) Chen, Z.; Koh, M.; Van Driessche, G.; Van Beeumen, J. J.; Bartsche, R. G.; Meyer, T. E.; Cusanovich, M. A.; Mathews, F. S. *Science* **1994**, *266*, 430−432.
(70) Ullmann, G. M.; Kostic, N. M. *J. Am. Chem. Soc.* **1995**, *117*, 4766−4774.
(71) Bjerrum, M. J.; Casimiro, D. R.; Chang, I.- J.; Di Bilio, A. J.; Gray, H. B.; Hill, M. G.; Langen, R.; Mines, G. A.; Skov, L. K.; Winkler, J. R.; Wuttke, D. S. *J. Bioenerg. Biomemb.* **1995**, *27*, 295−302.
(72) Beratan, D. N.; Onuchic, J. N.; Winkler, J. R.; Gray, H. B. *Science* **1992**, *258*, 1740−1741.
(73) Aquino, A. J. A.; Beroza, P.; Beratan, D. N.; Onuchic, J. N. *Chem. Phys.* **1995**, *197*, 277−288.
(74) Tiede, D. M.; Vashishta, A.; Gunner, M. R. *Biochem.* **1993**, *32*, 4515−4531.
(75) Gilson, M. K.; Honig, B. *Proteins: Struct., Funct., Genet.* **1988**, *3*, 32−52.
(76) Gilson, M. K.; Rashin, A.; Fine, R.; Honig, B. *J. Mol. Biol.* **1985**, *184*, 503−516.
(77) Honig, B.; Nicholls, A. *Science* **1995**, *268*, 1144−1149.
(78) Nicholls, A.; Honig, B. *J. Compu. Chem.* **1991**, *12*, 435−445.
(79) DelPhi and InsightII, Biosym, Inc., San Diego, CA.
(80) CONNOLY, Athay, Inc., 1994.
(81) Bosshard, H. R.; Anni, H.; Yonetoni, T. In *Peroxidases in Chemistry and Biology, Vol. II*; Everse, J.; Everse, K. E.; Grisham, M. B., Eds.; CRC Press: Boca Raton, FL, 1991; pp 51−84.
(82) Dawson, J. H. *Science* **1988**, *240*, 433−439.
(83) Yonetani, T. In *The Enzymes*; Boyer, P. D., Ed.; Academic Press: Orlando, FL, 1976; Vol. XIII, pp 345−361.
(84) Sivaraja, M.; Goodin, D. B.; Smith, M.; Hoffman, B. M. *Science* **1989**, *245*, 738−740.
(85) Houseman, A. L. P.; Doan, P. E.; Goodin, D. B.; Hoffman, B. M. *Biochemistry* **1993**, *32*, 4430−4443.
(86) Huyett, J. E.; Doan, P. E.; Gurbiel, R.; Houseman, A. L. P.; Sivaraja, M.; Goodin, D. B.; Hoffman, B. M. *J. Am. Chem. Soc.* **1995**, *117*, 9033−9041.
(87) Ho, P. S.; Hoffman, B. M.; Solomon, N.; Kang, C. H.; Margoliash, E. *Biochemistry* **1984**, *23*, 4122−4128.
(88) Ho, P. S.; Hoffman, B. M.; Kang, C. H.; Margoliash, E. *J. Biol. Chem.* **1983**, *258*, 4356−4363.
(89) Coulson, A. F. W.; Erman, J. E.; Yonetani, T. *J. Biol. Chem.* **1971**, *246*, 917−924.
(90) Hahm, S.; Geren, L.; Durham, B.; Millett, F. *J. Am. Chem. Soc.* **1993**, *115*, 3372−3373.
(91) Liu, R.; Miller, M. A.; Han, G. W.; Hahm, S.; Geren, L.; Hibdon, S.; Kraut, J.; Durham, B.; Millett, F. *Biochemistry* **1994**, *33*, 8678−8685.
(92) Summers, F. E.; Erman, J. E. *J. Biol. Chem.* **1988**, *263*, 14267−14275.
(93) Poulos, T. L.; Freer, S. T.; Alden, R. A.; Edwards, S. L.; Skogland, U.; Takio, K.; Eriksson, B.; Xuong, N.; Yonetani, T.; Kraut, J. *J. Biol. Chem.* **1980**, *255*, 575−580.
(94) Mochan, E. *Biochim. Biophys. Acta* **1970**, *216*, 80−95.
(95) Kang, C. H.; Brautigan, D. L.; Osheroff, N.; Margoliash, E. *J. Biol. Chem.* **1978**, *253*, 6502−6510.
(96) Koppenol, W. H.; Margoliash, E. *J. Biol. Chem.* **1982**, *257*, 4426−4437.
(97) Bechtold, R.; Bosshard, H. R. *J. Biol. Chem.* **1985**, *260*, 5191−5200.
(98) Poulos, T. L.; Kraut, J. *J. Biol. Chem.* **1980**, *255*, 10322−10330.
(99) Pelletier, H.; Kraut, J. *Science* **1992**, *258*, 1748−1755.
(100) Yi, Q.; Erman, J. E.; Satterlee, J. D. *Biochemistry* **1994**, *33*, 12032−12041.
(101) Jeng, Mei-F.; Englander, S. W.; Pardue, K.; Rogalskyj, J. S.; McLendon, G. *Nature Struct. Biol.* **1994**, *1*, 234−238.

(102) Hazzard, J. T.; Moench, S. J.; Erman, J. E.; Satterlee, J. D.; Tollin, G. *Biochemistry* **1988**, *27*, 2002−2008.
(103) Erman, J. E.; Kim, K. L.; Vitello, L. B.; Moench, S. J.; Satterlee, J. D. *Biochim. Biophys. Acta* **1987**, *911*, 1−10.
(104) Moench, S. J.; Satterlee, J. D.; Erman, J. E. *Biochemistry* **1987**, *26*, 3821−3826.
(105) Waldmeyer, B.; Bosshard, H. R. *J. Biol. Chem.* **1985**, *260*, 5184−5190.
(106) Wang, Y.; Margoliash, E. *Biochemistry* **1995**, *34*, 1948−1958.
(107) Pappa, H. S.; Poulos, T. L. *Biochemistry* **1995**, *34*, 6573−6580.
(108) Pappa, H. S.; Tajbaksh, S.; Saunders, A. J.; Pielak, G. J.; Poulos, T. L. *Biochem.* **1996**, *35*, 4837−4845.
(109) Northrup, S. H.; Boles, J. O.; Reynolds, J. C. L. *Science* **1988**, *241*, 67−70.
(110) Northrup, S. H.; Boles, J. O.; Reynolds, J. C. L. *J. Phys. Chem.* **1987**, *91*, 5991−5998.
(111) Northrup, S. H.; Thomasson, K. A. *FASEB J.* **1992**, *6*, A474.
(112) Northrup, S. H.; Reynolds, J. C. L.; Miller, C. M.; Forrest, K. J.; Boles, J. O. *J. Am. Chem. Soc.* **1986**, *108*, 8162−8170.
(113) Hazzard, J. T.; McLendon, G.; Cusanovich, M. A.; Tollin, G. *Biochem. Biophys. Res. Commun.* **1988**, *151*, 429−434.
(114) Nocek, J. M.; Liang, N.; Wallin, S. A.; Mauk, A. G.; Hoffman, B. M. *J. Am. Chem. Soc.* **1990**, *112*, 1623−1625.
(115) Nocek, J. M.; Stemp, E. D. A.; Finnegan, M. G.; Koshy, T. I.; Johnson, M. K.; Margoliash, E.; Mauk, A. G.; Smith, M.; Hoffman, B. M. *J. Am. Chem. Soc.* **1991**, *113*, 6822−6831.
(116) Wallin, S. A.; Stemp, E. D. A.; Everest, A. M.; Nocek, J. M.; Netzel, T. L.; Hoffman, B. M. *J. Am. Chem. Soc.* **1991**, *113*, 1842−1844.
(117) Kang, C. H.; Ferguson-Miller, S.; Margoliash, E. *J. Biol. Chem.* **1977**, *252*, 919−926.
(118) Mochan, E.; Nicholls, P. *Biochem. J.* **1971**, *121*, 69−82.
(119) Gupta, R. K.; Yonetani, T. *Biochim. Biophys. Acta* **1973**, *292*, 502−508.
(120) Leonard, J. J.; Yonetani, T. *Biochemistry* **1974**, *13*, 1465−1468.
(121) Erman, J. E.; Vitello, L. B. *J. Biol. Chem.* **1980**, *255*, 6224−6227.
(122) Vitello, L. B.; Erman, J. E. *Arch. Biochem. Biophys.* **1987**, *258*, 621−629.
(123) Corin, A. F.; McLendon, G.; Zhang, Q.; Hake, R. A.; Falvo, J.; Lu, K. S.; Ciccarelli, R. B.; Holzschu, D. *Biochemistry* **1991**, *30*, 11585−11595.
(124) Moench, S. J.; Chroni, S.; Lou, B.; Erman, J. E.; Satterlee, J. D. *Biochemistry* **1992**, *31*, 3661−3670.
(125) Everest, A. M.; Wallin, S. A.; Stemp, E. D. A.; Nocek, J. M.; Mauk, A. G.; Hoffman, B. M. *J. Am. Chem. Soc.* **1991**, *113*, 4337−4338.
(126) Zhou, J. S.; Hoffman, B. M. *Science* **1994**, *265*, 1693−1696.
(127) McLendon, G.; Zhang, Q.; Wallin, S. A.; Miller, R. M.; Billstone, V.; Spears, K. G.; Hoffman, B. M. *J. Am. Chem. Soc.* **1993**, *115*, 3665−3669.
(128) DeVan; Hoffman, B. M. (1996): Unpublished results.
(129) Zhou, J. S.; Nocek, J. M.; DeVan, M. L.; Hoffman, B. M. *Science* **1995**, *269*, 204−207.
(130) Mauk, M. R.; Ferrer, J. C.; Mauk, A. G. *Biochemistry* **1994**, *33*, 12609−12614.
(131) Matthis, A. L.; Erman, J. E. *Biochemistry* **1995**, *34*, 9985−9990.
(132) Matthis, A. L.; Vitello, L. B.; Erman, J. E. *Biochemistry* **1995**, *34*, 9991.
(133) Miller, M. A.; Geren, L.; Han, G. W.; Saunders, A.; Beasley, J.; Pielak, G. J.; Durham, B.; Millett, F.; Kraut, J. *Biochemistry* **1996**, *35*, 667−673.
(134) Yi, Q.; Erman, J. E.; Satterlee, J. D. *J. Am. Chem. Soc.* **1992**, *114*, 1901−1909.
(135) Yi, Q.; Erman, J. E.; Satterlee, J. D. *Biochemistry* **1993**, *32*, 10988−10994.
(136) Satterlee, J. D.; Moench, S. J.; Erman, J. E. *Biochim. Biophys. Acta* **1987**, *912*, 87−97.
(137) Yi, Q.; Erman, J. E.; Satterlee, J. D. *J. Am. Chem. Soc.* **1994**, *116*, 1981−1987.
(138) Hildebrandt, P.; English, A. M.; Smulevich, G. *Biochemistry* **1992**, *31*, 2384−2392.
(139) Wang, J.; Larsen, R. W.; Moench, S. J.; Satterlee, J. D.; Rousseau, D. L.; Ondrias, M. R. *Biochemistry* **1996**, *35*, 455−465.
(140) Anni, H.; Vanderkooi, J. M.; Sharp, K. A.; Yonetani, T.; Hopkins, S. C. *Biochemistry* **1994**, *33*, 3475−3486.
(141) Smulevich, G.; Mauro, J. M.; Fishel, L. A.; English, A. M.; Kraut, J.; Spiro, T. G. *Biochemistry* **1988**, *27*, 5477−5485.
(142) Goodin, D. B.; Davidson, M. G.; Roe, J. A.; Mauk, A. G.; Smith, M. *Biochemistry* **1991**, *30*, 4953−4962.
(143) Miller, M. A.; Mauro, J. M.; Smulevich, G.; Coletta, M.; Kraut, J.; Traylor, T. G. *Biochemistry* **1990**, *29*, 9978−9988.
(144) Fishel, L. A.; Villafranca, J. E.; Mauro, J. M.; Kraut, J. *Biochemistry* **1987**, *26*, 351−360.
(145) Smulevich, G.; Wang, Y.; Mauro, J. M.; Wang, J.; Fishel, L. A.; Kraut, J.; Spiro, T. G. *Biochemistry* **1990**, *29*, 7174−7180.
(146) Smulevich, G.; Mauro, J. M.; Fishel, L. A.; English, A. M.; Kraut, J.; Spiro, T. G. *Biochemistry* **1988**, *27*, 5486−5492.
(147) Sundaramoorthy, M.; Choudhury, K.; Edwards, S. L.; Poulos, T. L. *J. Am. Chem. Soc.* **1991**, *113*, 7755−7757.
(148) Hahm, S.; Miller, M. A.; Geren, L.; Kraut, J.; Durham, B.; Millett, F. *Biochemistry* **1994**, *33*, 1473−1480.
(149) Miller, M. A.; Vitello, L.; Erman, J. E. *Biochemistry* **1995**, *34*, 12048−12058.
(150) Miller, M. A.; Hazzard, J. T.; Mauro, J. M.; Edwards, S. L.; Simons, P. C.; Tollin, G.; Kraut, J. *Biochemistry* **1988**, *27*, 9081−9088.
(151) Erman, J. E.; Vitello, L. B.; Mauro, J. M.; Kraut, J. *Biochemistry* **1989**, *28*, 7992−7995.
(152) Miller, M. A.; Bandyopadhyay, D.; Mauro, J. M.; Traylor, T. G.; Kraut, J. *Biochemistry* **1992**, *31*, 2789−2797.
(153) Ferrer, J. C.; Turano, P.; Banci, L.; Bertini, I.; Morris, I. K.; Smith, K. M.; Smith, M.; Mauk, A. G. *Biochemistry* **1994**, *33*, 7819−7829.
(154) Hake, R.; McLendon, G.; Corin, A.; Holzschu, D. *J. Am. Chem. Soc.* **1992**, *114*, 5442−5443.
(155) Miller, M. A.; Liu, R.; Hahm, S.; Geren, L.; Hibdon, S.; Kraut, J.; Durham, B.; Millett, F. *Biochemistry* **1994**, *33*, 8686−8693.
(156) Corin, A. F.; Hake, R. A.; McLendon, G.; Hazzard, J. T.; Tollin, G. *Biochemistry* **1993**, *32*, 2756−2762.
(157) Mauk, A. G. *Struct. Bonding* **1991**, *75*, 131−157.
(158) Fitzgerald, M. M.; Churchill, M. J.; McRee, D. E.; Goodin, D. B. *Biochemistry* **1994**, *33*, 3807−3818.
(159) Fishel, L. A.; Farnum, M. F.; Mauro, J. M.; Miller, M. A.; Kraut, J.; Liu, Y.; Tan, X.; Scholes, C. P. *Biochemistry* **1991**, *30*, 1986−1996.
(160) Scholes, C. P.; Liu, Y.; Fishel, L. A.; Farnum, M. F.; Mauro, J. M.; Kraut, J. *Isr. J. Chem.* **1989**, *29*, 85−92.
(161) Mauro, J. M.; Fishel, L. A.; Hazzard, J. T.; Meyer, T. E.; Tollin, G.; Cusanovich, M. A.; Kraut, J. *Biochemistry* **1988**, *27*, 6243−6256.
(162) Goodin, D. B.; McRee, D. E. *Biochemistry* **1993**, *32*, 3313−3324.
(163) Liu, R.; Hahm, S.; Miller, M.; Durham, B.; Millet, F. *Biochemistry* **1995**, *34*, 973−983.
(164) Wang, J.; Mauro, J. M.; Edwards, S. L.; Oatley, S. J.; Fishel, L. A.; Ashford, V. A.; Xuong, N.; Kraut, J. *Biochemistry* **1990**, *29*, 7160−7173.
(165) Patterson, W. R.; Poulos, T. L. *Biochemistry* **1995**, *34*, 4331−4341.
(166) Bonagura, C. A.; Sundaramoorthy, M.; Pappa, H. S.; Patterson, W. R.; Poulos, T. L. *Biochemistry* **1996**, *35*, 6107−6115.
(167) Zhou, J. S.; Tran, S.; McLendon, G.; Hoffman, B. M., unpublished results, 1996.
(168) Hazzard, J. T.; Tollin, G. *J. Am. Chem. Soc.* **1991**, *113*, 8956−8957.
(169) Nuevo, M. R.; Chu, H.; Vitello, L. B.; Erman, J. E. *J. Am. Chem. Soc.* **1993**, *115*, 5873−5874.

CR9500444